January 2023

# Evaluation Of Water Content Measurement Model 3000 Probe (wcm-3000) Using The NASA Impacts Dataset

Jennifer Rose Moore

# EVALUATION OF WATER CONTENT MEASUREMENT MODEL 3000 PROBE (WCM-3000) USING THE NASA IMPACTS DATASET

by

Jennifer Rose Moore
Bachelor of Science, Millersville University, 2021

A Thesis

Submitted to the Graduate Faculty

of the

University of North Dakota

in partial fulfillment of the requirements

for the degree of
Master of Science

Grand Forks, North Dakota

December 2023

This thesis, submitted by Jennifer Moore in partial fulfillment of the requirements for the Degree of Master of Science from the University of North Dakota, has been read by the Faculty Advisory Committee under whom the work has been done and is hereby approved.

_____
David Delene, Committee Chair

_____
Michael Poellot, Committee Member

_____
Jared Marquis, Committee Member

This thesis is being submitted by the appointed advisory committee as having met all of the requirements of the School of Graduate Studies at the University of North Dakota and is hereby approved.

_____
Dr. Chris Nelson, Dean
School of Graduate Studies

_____
DATE

PERMISSION

| | |
|---|---|
| Title | Evaluation of Water Content Measurement Model 3000 Probe (WCM-3000) Using the NASA IMPACTS Dataset |
| Department | Atmospheric Sciences |
| Degree | Master of Science |

In presenting this thesis in partial fulfillment of the requirements for a graduate degree from the University of North Dakota, I agree that the library of this University shall make it freely available for inspection. I further agree that permission for extensive copying for scholarly purposes may be granted by the professor who supervised my thesis work or, in her absence, by the Chairperson of the department or the dean of the School of Graduate Studies. It is understood that any copying or publication or other use of this thesis or part thereof for financial gain shall not be allowed without my written permission. It is also understood that due recognition shall be given to me and to the University of North Dakota in any scholarly use which may be made of any material in my thesis.

Jennifer R. Moore
January 30, 2023

# Table of Contents

# LIST OF FIGURES

# LIST OF TABLES

## ACKNOWLEDGEMENTS

Thank you to David Delene, Michael Poellot, and Jared Marquis, who reviewed the content and provided supplementing information and guidance. Thank you to Andrew Detwiler for contributing wisdom on aircraft instrumentation and microphysics. Thank you to Christian Nairy for working beside me on the IMPACTS 2022 and 2023 Field Campaign and sharing wisdom on aircraft instrumentation. Thank you to Michael Willette for working with me in the lab, on the 2023 IMPACTS Field Campaign and always being supportive. Thank you to my friends and family who have supported me throughout this process. Funding for this study was provided by NASA grant 43500-2210-UND0023042.

# ABSTRACT

The introduction of the Water Content Measurement probe (WCM-3000) onto the NASA P-3 aircraft during the NASA Investigation of Microphysics and Precipitation for Atlantic Coast-Threatening Snowstorms (IMPACTS) 2022 and 2023 field campaign raises opportunity for measurement comparisons between liquid water content instruments. Instrument comparisons are done between the King hot-wire probe, the WCM-3000, and the Cloud Droplet Probe (CDP) using the IMPACTS 2023 field campaign data. Case studies are analyzed in three cloud conditions; liquid water clouds with droplets less than 50 μm, supercooled liquid water clouds with droplets less than 50 μm, and ice phase clouds. The WCM-3000 and King Probe did not agree within measurement uncertainties. Possible WCM-3000 issues are a time-offset, a hysteresis effect and an overdamped control system. Analysis indicates that likely the WCM is overdamped, and discussion is on-going with the manufacturer regarding the WCM performance.

# CHAPTER I

# INTRODUCTION

The NASA Investigation of Microphysics and Precipitation in Atlantic Coast Threatening Snowstorms (IMPACTS) campaign was performed during the winters of 2020, 2022, and 2023 to better understand the precipitation process of winter storms (L. A. McMurdie et al., 2022). Cloud physics processes within winter storms remains obscure due to the lack of in-situ observations and limitations of remote sensing capabilities. The banded structure of snow storms observed by remote sensing instruments, such as radars, is related to dynamic and microphysical processes. An important microphysical parameter is liquid water content (LWC), which is defined as the amount of liquid water contained in a unit volume of air. While the King hot-wire probe (King et al., 1978) has been used for aircraft LWC measurements since the 1970's, newer instruments are being implemented in airborne research. During the 2022 and 2023 field campaign, LWC was measured using a King hot-wire probe, a Water Content Measurement (WCM; Lilie et al., 2016, 2021) model 3000 probe, and a Cloud Droplet Probe (CDP; Lance et al., 2010) on the NASA P-3 research aircraft platform. Measuring LWC with several probes allows for inter-comparisons which can be used to improve our interpretation of LWC measurements.

LWC is a valuable microphysics parameter used in many scientific studies and aircraft icing certifications. To mitigate fatal aircraft icing scenarios, icing certifications are performed on the aircraft frame and engine. One way to certify aircraft parts is by using icing tunnels. Icing tunnels use hot-wire probes and other microphysics instruments as a way to check the performance of aircraft parts during simulated icing events. For this reason, it is important that hot-wire probes measure water contents adequately. Additionally, LWC measurements can be used for verification purposes in model studies. Many model verification studies compare in-situ LWC measurements

to model simulated data as a way to test the model's ability to create a realistic outcome. One example of model verification through in-situ measurements is Sandvik et al., 2007, where model runs of Artic mixed phased clouds had underrepresented LWC and overrepresented IWC.

*Liquid Water Content Measurements*

The implementation of hot-wire probes onto airborne research platforms dates back to the 1950's (Strapp et al., 2003). Hot-wire probes were created to measure liquid water content by modifying the design of hot-wire anemometers that were originally used to measure wind turbulence. One of the first widely used LWC probes was the Johnson-Williams (JW) hot-wire probe (Figure 1), which used constant electrical current to measure liquid water (King et al., 1978). A short-coming of the JW probe was its narrow droplet size range detected, meaning droplets larger than 30 µm were not measured (Merceret & Schricker, 1975). In the late 1970's, the Particle Measurement Systems (PMS) King probe was introduced as a constant-temperature probe, which provided easier interpretation and no requirement for a wet calibration, which was necessary with the JW probe (King et al., 1978).

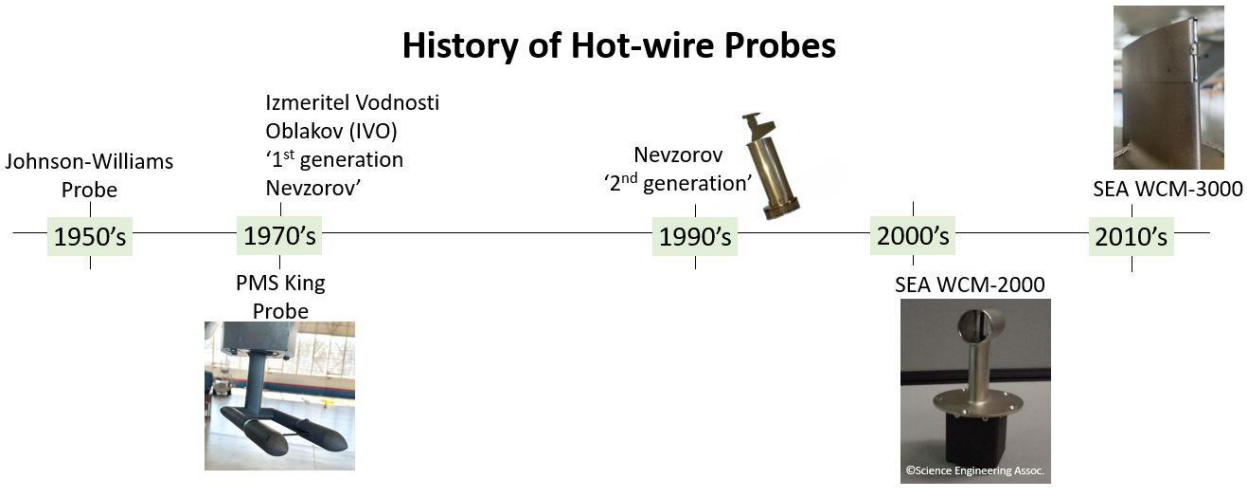


Figure 1: Hot-wire probe history dating back to the 1950's with the Bacharach Instrument Company's Johnson-Williams Probe.

Liquid water and ice particles behave differently when encountering hot-wires. Small liquid droplets interact with the wire by flattening into a thin film which quickly evaporates (A. V. Korolev et al., 1998). Unlike liquid droplets, ice particles deflect off the wire. Thus, when using the JW and King probes, cloud measurements were primarily sensitive to liquid droplets and not cloud ice. Therefore, in the 1970's, the only measurements of total water contents (TWC) – that is the total equivalent water held in liquid and solid hydrometeors – were done using imaging probes (Brown & Francis, 1995) or the Ruskin probe (Personne et al., 1982). The Nevzorov probe demonstrated a design to measure total water contents (TWC) by using a conical shaped sensor that collects both water and ice particles. The sensor shape allows for both the liquid and ice particle to be aerodynamically contained within the conical shaped sensor while the particles are heated to evaporation (A. V. Korolev et al., 1998). With the measurement of both LWC and TWC, ice water content (IWC) can be derived by subtracting the measured LWC from TWC.

Smaller wire diameters were originally believed to have a smaller collection efficiency when larger droplets are present due to the wire size not being able to intercept the larger droplets. In Lilie et al. (2005), model runs have shown droplets greater than 30 μm were able to be collected by any wire regardless of its shape or size. Therefore, it is likely that the issue is related to the wire not being able to retain the larger droplets before the wire evaporates it (Lilie et al., 2005). Science Engineering Associates (SEA) created a multi-wire probe with this principle in mind. The SEA Multi-Element Water Content system, model 2000 (WCM-2000) has four sensing elements: TWC; LWC-083; LWC-021; and a compensation element. The two LWC sensors have different wire diameter sizes allowing for a distinction in the droplet diameter of the sampled LWC. Because the WCM-2000 measures both LWC and TWC, the degree of glaciation of a cloud can be determined. Glaciation refers to the process by which liquid droplets transform into ice particles, an integral

step in phase change for mixed-phase clouds (A. Korolev & Isaac, 2003). In ice only clouds (clouds that are completely glaciated), the TWC element will have the highest response while the LWC element will be near zero. In mixed phase clouds, where there is some degree of glaciation, both TWC and LWC elements will respond. In liquid only clouds with no degree of glaciation, all wires will respond with the variation in responses due to the droplet diameter size retention for the varying wire sizes. Additionally, the WCM-2000 used a compensation element to account for heat loss in the wire from airflow. To minimize the heat loss from LWC, the compensation element is oriented along the direction of flight. The SEA Water Content system, model 3000 (WCM-3000) is used in this study and explained in Chapter 3.

Other methods to measure cloud water contents include the use of imaging probes and forward scattering probes. LWC can be derived by integrating the droplet distribution measured with probes such as the Droplet Measurement Technologies Forward Scattering Spectrometer Probe (FSSP; Dye & Baumgardner, 1984) and CDP. However, these estimates may be limited due to limitations in measured droplet size ranges and frequency of measurements. Studies have also been conducted to measure high IWC conditions with an isokinetic evaporator (Lilie, 2021). The Rosemount Icing Detector (RICE; Claffey et al., 1995) is also used to measure supercooled liquid water (SCLW).

*Thesis Objectives*

Instrument comparisons allow for the determination of any instrument limitations as well as the interpretation of measurements from different probes. As widely used probes go out of production, comparisons of measurement uncertainties can provide historical preservation of LWC measurements. Since the WCM-3000 is a new probe for the NASA P-3, it is important to compare measurements taken during the 2022 and 2023 field campaign with the other cloud physics probes on the P-3. To make the comparisons, three cloud conditions are defined. The three conditions are

LWC clouds, SCLW clouds with no ice, and mixed phase clouds. The overall objective is to determine if the WCM-3000 values agree with other probes within their measured uncertainties. This comparison is made using the NASA IMPACTS field campaign data set.

# CHAPTER II

# DATASET

*NASA IMPACTS Field Campaign*

The overarching goal of NASA IMPACTS is to better understand the structure of winter storms through in-situ and remote sensing observations. Dynamical, thermodynamic, and microphysical processes are studied using in-situ aircraft, remote sensing aircraft, and ground observations (L. A. McMurdie et al., 2022). With the use of co-located ER-2 and P-3 aircraft, the IMPACTS project collected detailed microphysics and cloud structures simultaneously. The NASA P-3 aircraft has a variety of in-situ instruments for collecting microphysical data and environmental conditions. The NASA ER-2 aircraft has a suite of remote sensing instruments used to measure cloud data from above. Coordinated flight legs between the two aircraft allow both planes to sample the same region of clouds from multiple observing locations. This coordination can provide verification of what cloud particle habits and concentrations the remote sensing instruments are measuring to assist in other situations where in-situ observations are unavailable (e.g. satellite observations).

*Aircraft In-situ Instrument Platform*

The NASA P-3 was stationed out of Wallops Island Flight Facility during the NASA IMPACTS field campaign. The cloud microphysical instruments onboard the NASA P-3 included imaging probes, hot-wire probes, forward scattering probes, and vibrating cylinders. Measurement size ranges differ between instruments allowing for overlap of particle sizes from 2 μm to 19.2 millimeters. Forward scattering probes distinguish particle diameters, particle concentrations, and LWC. Hot-wire probes are used to measure cloud water contents (CWC's); ie. LWC, TWC, and IWC. There were several types of imaging probes deployed on the P-3. The Hawkeye-Cloud Particle Imager (CPI) and Particle Habit Imaging and Polar Scattering probe (PHIPS) are mainly used to distinguish particle habits at a high resolution. The 2-Dimensional Stereo probe (2D-S,

Lawson et al., 2006) and the High Volume Precipitation Spectrometer version 3 (HVPS-3) are also imaging probes but are mainly used to obtain particle concentrations and sizes. A vibrating cylinder instrument is used to distinguish periods of icing when super cooled liquid water is present. The 2022 field campaign conducted a total of 14 P-3 flights, 2 calibration flights and 12 science flights. The 2023 field campaign conducted a total of 18 P-3 flights, consisting of 5 calibration flights and 13 science flights.

Mounted under the left wing of the P-3, the hot-wire boom (Figure 2) houses 4 microphysical instruments orthogonal to a pitot tube. The pitot tube extends beyond the leading edge of the wing, with the WCM-3000, King, CDP, and the RICE-B mounted on the top, bottom, right, and left, respectively. The hot-wire boom allows for the instruments to be measured in close proximity to one another, which provides less error assuming that the P-3 is penetrating a uniform cloud.

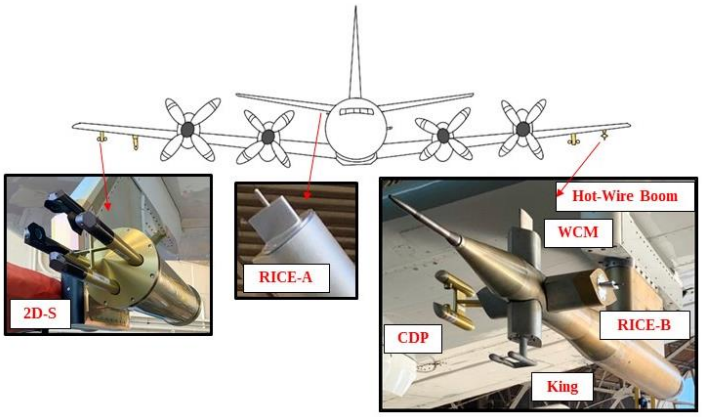


Figure 2 The placement of wing pylons housing the University of North Dakota operated microphysics probes on the NASA P-3 aircraft. The Hot-wire boom pylon houses the Water Content Measurement probe, Cloud Droplet Probe, King probe, and the Rosemount Icing detector – B (2023). The 2-Dimensional Stereo Probe is on the right wing of the P-3 aircraft. The Rosemount icing detector – A is on the Fuselage.

When interpreting in-situ microphysics datasets, it is important to understand the instruments measurement size ranges. Different instruments measure different particle sizes depending on the measurement method. The size ranges, sampling frequency, and measurement methods of the different probes analyzed in this study are summarized in Table 1. The Cloud Droplet Probe (CDP)

uses forward scattering to measure cloud droplets between 2 and 50 μm as they pass through the optical field created by the laser and detector (Lance et al., 2010). As droplets pass through the optical field of the CDP the droplet scatters the laser. Droplets that scatter light within an angle of 4 - 12° towards the detector are sampled. This scattered light is then used to estimate droplet size and droplet size distribution. The CDP integrates the droplet distribution to get LWC. Equation 1 is used to calculate LWC from the CDP; where $n_i$ is the number of particles in each bin, $\rho_w$ is the density of water, and d is the droplet diameter.

$$\mathrm{LWC} = \sum \mathrm{n_i}\ \rho_w \pi \frac{d^3}{6} \tag{1}$$

The Spec Inc. Two-Dimensional Stereo Probe (2D-S, Lawson et al., 2006) and the Collins Aerospace Rosemount Icing Detector (RICE) are used to determine cloud conditions. The 2D-S is an optical imaging probe that uses orthogonal lasers to sample cloud particles. As cloud particles pass in front of the laser beams, a shadow is casted onto the 128-photodiode arrays resulting in an image of the cloud particle (Lawson et al., 2006). The RICE probe is a vibrating cylinder which measures super-cooled liquid water (SCLW). SCLW freezes on contact with cloud particles, aircraft frames, etc. The RICE probe vibrates at a specific frequency and as SCLW accretes on the metal vibrating cylinder, the vibration frequency dampens.

Table 1. Microphysical instruments on the NASA IMPACTS field project for the 2022 and 2023 winters. Important parameters for the Water Content Measurement probe (WCM-3000), King Hot-wire probe (King), and the Cloud Droplet Probe (CDP) are provided. The frequency is that of the raw recorded data file, which is the highest frequency available. The 2D-S size range is based on having 128 diodes, 10 μm each; however, the image processing methodology and configuration determines the exact size range.

| **Instrument** | **Frequency** | **Size Range** | **Measurement Method** |
|---|---|---|---|
| WCM-3000 | 1 *Hz* | 5-200 μm | Hot-wire |
| King | *25 Hz* | 5-200 μm | Hot-wire |
| CDP | *10 Hz* | 2-50 μm | Forward Scattering |
| RICE | *4 Hz* | N/A | Vibrating Cylinder |
| 2D-S | *1 Hz* | 10 μm - 1.280mm | Imaging Probe |

# CHAPTER III

# INSTRUMENTATION

*Hot-wire Probes*

The hot-wire probe sensing element is maintained at a specific temperature by suppling enough power. The total power ($P_{total}$) supplied is divided into a dry ($P_{dry}$) and wet ($P_{wet}$) term, which is represented by the equation:

$$P_{total} = P_{dry} + P_{wet} \tag{2}$$

The dry term includes heat loss from mechanisms that cool the wire other than the evaporation of water. Airflow affects the dry term to the largest extent; however, the dry term incorporates any heat loss from conduction, radiation, and convection. The wet term refers to heat loss due to the evaporation of water. Heat loss from radiation and conduction is minimized for the WCM-3000 by adding an insulating spacer (Figure 3) between the sensor and strut (Lilie et al., 2016, 2021). The largest component of the dry term is convection. Convective heat transfer is the heat loss from the movement of a fluid – air in this case. To calculate the dry term the use of ambient conditions (airspeed, altitude, and air temperature) is used to simulate being in a cloud-free environment, with the equation given as,

$$P_{dry} = C_1 \times (T_{wire} - T_{air}) \times (TAS \times P_{static})^k \tag{3}$$

Where $C_1$, and k are constants, $T_{wire}$ is the temperature of the sensing element, $T_{air}$ is the static air temperature, TAS is the true air speed, and $P_{static}$ is the static pressure. The dry power can also be calculated with ambient air density instead of static pressure, to get a more accurate measured value using the equation,

$$P_{dry} = C_1 \times (T_{wire} - T_{air}) \times (TAS \times pv)^k \tag{4}$$

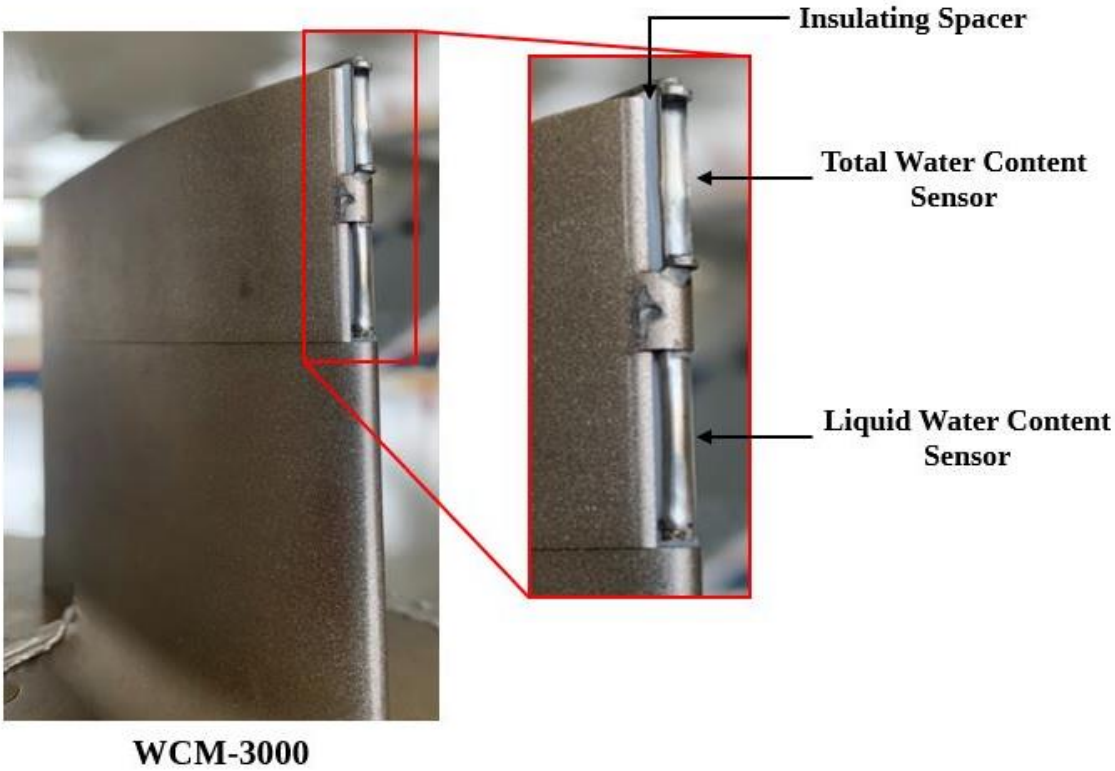


Figure 3: Image showing the Water Content Measurement model 3000 (WCM-3000) probe. The total water content (TWC) sensor is concave and the liquid water content (LWC) sensor is convex. Insulating spacers are used between the sensor and strut to minimize heat loss.

The wet term represents the change in sensor power due to the evaporation of intercepted water. After the sensor intercepts water, the droplet at ambient air temperature is heated to the evaporative temperature, where the droplet changes phase. In addition to the heat required to raise the temperature to the evaporative temperature, an additional amount of heat, equal to the latent heat of evaporation, is needed to fully evaporate the droplet. Latent heat of evaporation is the amount of energy required for water to change phases while keeping temperature and pressure constant.

LWC can be calculated by

$$LWC\ \left(\frac{g}{m^3}\right) = \frac{P_{sense,wet}\,(W) * 2.389x10^5}{\left[L_{evap}\left(\frac{cal}{g}\right) + 1.0\left(\frac{cal}{g°C}\right) * (T_{evap} - T_{amb})\right] * TAS\left(\frac{m}{s}\right) * l_s(mm) * W_s(mm)} \quad (5)$$

Where $P_{sense,wet}$ is the power of the wet sensor, $L_{evap}$ is the latent heat of evaporation, $T_{evap}$ is the evaporative temperature, $T_{amb}$ is the ambient temperature, TAS is the true air speed, $l_s$ is the length of the sensor, and $W_s$ is the width of the sensor. TWC can be calculated with the same equation as LWC by using latent heat of fusion.

*WCM-3000 Specifications*

The second generation of the SEA Water Content System Model 3000 (WCM-3000) has two sensors: one to measure LWC and the other to measure TWC. Unlike the WCM-2000 design, the WCM-3000 has a heated metal strut that holds a concave TWC sensor and a convex LWC sensor. According to SEA, this design allows for ice crystal detection. However, it is important to note that, TWC and LWC sensors are both sensitive to LWC but not IWC. The LWC sensor exhibits some residual sensitivity to ice crystals and the TWC sensor cannot always aerodynamically contain all ice crystals (Lilie et al., 2016). Due to the maximum power consumption of the WCM being 49 amps, LWC and TWC can be measured up to 10 $g/m^3$ at TAS less than 150 $ms^{-1}$ and 6 $g/m^3$ for TAS between 150 $ms^{-1}$ and 230 $ms^{-1}$ (Science Engineering Associates, n.d.). The WCM-3000 has a smaller surface area than the King and WCM-2000 probes. The difference in wire sizes, temperatures, wire type (coiled/uncoiled), and power consumption are listed in Table 2. During the 2022 NASA IMPACTS field project, the WCM-3000 was introduced for the first time on the NASA P-3 aircraft.

Table 2. Hot-wire element sizes, wire temperature (temp), wire type, and power used to evaporate 1.0 $g/m^3$ water at 0°C, true air speed of 130$ms^{-1}$, and at 600 hPa. Verified with ADPAA code to conform with table.

| Instrument | Element | Width | Length | Temp. | Area | Coiled | Power |
|---|---|---|---|---|---|---|---|
| WCM-3000 | LWC | 2.39 mm | 10.01 mm | 140 °C | 23.89 $mm^2$ | No | 1.64 W |
| WCM-3000 | TWC | 2.44 mm | 10.01 mm | 140 °C | 24.40 $mm^2$ | No | 1.67 W |
| King | LWC | 2.06 mm | 20.00 mm | 185 °C | 39.00 $mm^2$ | Yes | 2.68 W |
| WCM-2000 | 083 LWC | 2.11 mm | 22.38 mm | 140 °C | 47.18 $mm^2$ | No | 3.24 W |
| WCM-2000 | 021 LWC | 0.53 mm | 21.77 mm | 140 °C | 11.61 $mm^2$ | No | 0.80 W |

| | | | | | | | |
|---|---|---|---|---|---|---|---|
| WCM-2000 | TWC | 2.11 mm | 23.06 mm | 140 °C | 48.62 $mm^2$ | No | 3.34 W |
| WCM-2000 | Comp | 0.28 mm | 16.76 mm | 140 °C | 4.68 $mm^2$ | No | N/A |
| Nevzorov | LWC | 2.10 mm | 16.30 mm | 140 °C | 34.23 $mm^2$ | Yes | 2.35 W |
| Nevzorov | TWC | 8.00 mm | N/A | 140 °C | 50.20 $mm^2$ | Yes | 3.44 W |

*Data Processing*

Airborne Data Processing and Analysis (ADPAA) is an open source processing package created to automate data processing procedures (Delene, 2011). Post processed output files are comprised of data stream files and summary files. Data stream files output all collected parameters from the probe, such as power supplied to instrument, sensor temperature, and calculated parameters such as LWC. Summary files contain relevant parameters for each instrument implemented during a field campaign. During post processing, calibrations and corrections will be applied to relevant instruments before quality assurance is done. Quality assurance is done by removing rogue data points in the dataset.

*Corrections*

Another step taken during post processing is applying corrections to the hot-wire probes. Hot-wire probe LWC measurements have been known to deviate in periods of out-of-cloud time segments as well as clear air maneuvers. Changes in pressure and temperature during flight results in changes in the dry term calculation. Deviations in the dry term during out of cloud time periods are adjusted in post processing. The adjustment is done so the out of cloud LWC is zero. The hot-wire LWC measurements are computed before the FSSP/CDP concentrations deem out-of-cloud time segments. For aircraft instrumentation purposes, a cloud is defined as a 1 $km^2$ parcel. At the edge of cumulus clouds, there are fractus clouds, which are remnants of dissipated clouds. This definition provides the basis for the fractus clouds at the edges of cumulus clouds to not be interpreted. For the NASA P-3 aircraft, it is interpreted that it would take 10 seconds to fly 1 km. The FSSP/CDP cloud time interval is 10 seconds for this reason. Corrections are applied to account

for deviations in LWC based on measurements from the FSSP/CDP. The FSSP/CDP is used to distinguish in cloud time intervals. A buffer is applied to the time period determined by the FSSP/CDP. This buffer differs depending on the aircraft. For the NASA P-3 the buffer time period is considered 10 seconds. This buffer is added on to the time before and after the FSSP/CDP determines the plane as in cloud. The cloud time interval and buffer parameters change depending on the aircraft and field campaign. For the IMPACTS field campaign, the King and WCM-3000 parameters are listed in Table 3.

Table 3. FSSP cloud time interval and buffer parameters used in ADPAA processing code for the King and Water Content Measurement probe (WCM-3000)

| **Instrument** | **Cloud Time Interval** | **Buffer time period** |
|---|---|---|
| King | 10 | 1.0 |
| WCM-3000 | 10 | 1.0 |

# CHAPTER IV

# METHODOLOGY

*Calibrations*

Ideally, instrument calibrations should be consistent between the beginning and end of each field campaign, though calibration coefficients can change due to instrument damage or contamination. Thus, calibrations should be done at the beginning and end of each field campaign to ensure that the calibration coefficients are relatively the same. ADPAA applies the calibrations in post processing for both the King and WCM. Post campaign calibrations are explained here for the WCM-3000. Calibration coefficients are determined by using clear air speed runs. Using the dry term equation, the calibration constants (C1, C2, and k in Eq. 3) are found. Note, the k coefficient is typically a value around 0.5 (Lilie et al., 2021). Solving for the constants in equation 3, clear air speed run data are plotted on a graph. An easier way to interpret the dry term equation is to put it in this form,

$$P_{element} = C_1 + C_2 X \tag{6}$$

where $X = (T_{wire} - T_{air}) * (TAS * P_{static})^k$. In this form it is easy to determine the coefficients since the equation is linear, y = mx + b. The measured clear air speed run values are now encompassed by the term X. By plotting X on the x-axis and $P_{element}$ on the y-axis the data takes on a linear form where constants C1 is the y-intercept and C2 is the slope.

To properly determine the calibration coefficients, the plane must vary airspeed without varying other parameters such as static pressure and static temperature during the clear air speed run. This can be accomplished by varying airspeed while maintaining a constant altitude in clear air. During the IMPACTS 2023 calibration flights, clear air speed runs were performed at multiple altitudes. The P-3 increases and decreases its TAS at one altitude before climbing to the next

altitude to performing the same procedure. Speed run segment times were found by plotting TAS and LWC to determine clear air times. Each constant altitude segment is then determined through examination of TAS and altitude. When determining the length of the segments, heading turns, rolls, and large altitude deviations, are often found at the beginning and end of the speed run time and are avoided. It is important to note that several segments of speed run times with differing altitudes are used to determine if there is variation in the coefficients based on the altitude.

Figure 4 shows the TAS and altitude for the 12 December 2022 calibration flight. Four clear air speed runs at constant altitude are indicated. The time periods, TAS, temperatures, altitudes and pressures for each clear air speed run are summarized in Table 4.

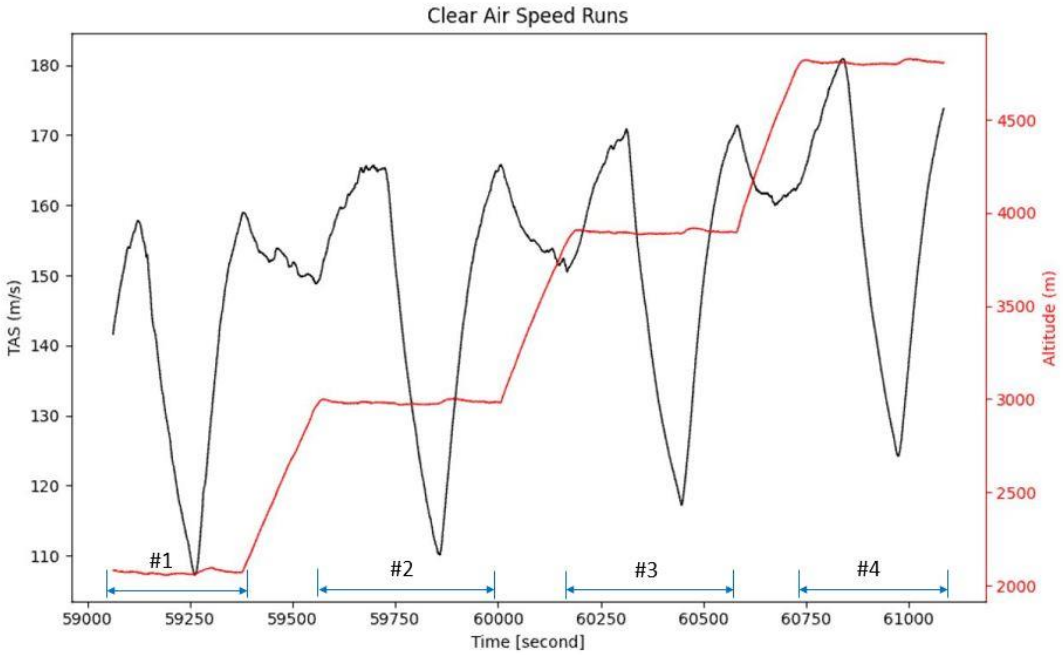


Figure 4: Clear air speed run maneuvers performed by the NASA P-3 on 12 December 2022 flight.

Table 4. List of time periods for the 4 clear air speed run maneuvers conducted on 12 December 2022 IMPACTS flight. Described are the start and end time of each speed run, the lowest and highest speed, average temperature (temp), average altitude, and average pressure (press).

| Date | Start Time | End Time | Speeds | Temp. | Altitude | Press. |
|---|---|---|---|---|---|---|
| 20221212 | 16:24:21 UTC | 16:29:27 UTC | 107-157 kts | -5.6 °C | 2000 m | 788 hPa |
| 20221212 | 16:35:37 UTC | 16:39:40 UTC | 110-165 kts | -10.4 °C | 2900 m | 702 hPa |
| 20221212 | 16:43:27 UTC | 16:49:04 UTC | 117-170 kts | -16.5 °C | 3900 m | 624 hPa |

| | | | | | | |
|---|---|---|---|---|---|---|
| 20221212 | 16:54:47 UTC | 16:58:06 UTC | 124-174 kts | -22.0 °C | 4800 m | 554 hPa |

*Speed Run Data Analysis*

Speed run data are analyzed to find the WCM-3000 calibration coefficients, which are applied in post processing for the dry term. A linear regression is plotted for both the LWC and TWC element using the clear air speed runs at the four altitudes. The linear regressions show similar trend lines between the altitudes analyzed (Figure 5 and Figure 6). There is little change in slope and y-intercept between the altitudes for both the LWC and TWC element. This means that the change in altitude does not greatly affect the calibration coefficients. The R squared values of both the LWC and TWC element show the line of best fit is representative of the data. Since the data processing code needs one set of coefficients, and since the trend lines are similar (Figure 7), only one altitude is used for the calibration coefficients. A typical flight altitude for IMPACTS science flights was 2900 m, where LWC and TWC are often sampled in winter storms. Therefore, coefficients from altitude 2900 m are applied to the dry term for the LWC and TWC elements. The LWC coefficients for C1 and C2 are 1.78 and $2.38e^{-05}$ respectively. The TWC coefficients for C1 and C2 are 2.87 and $1.47e^{-05}$ respectively.

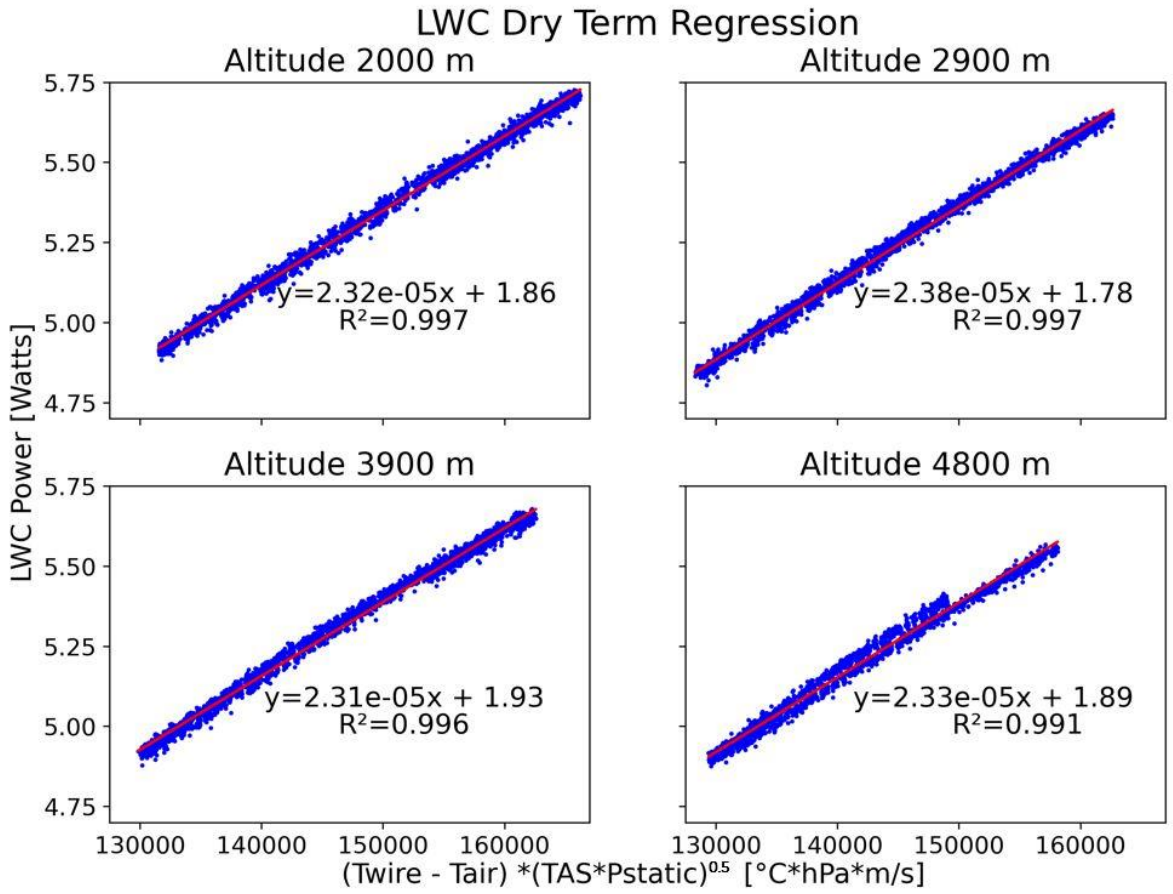


Figure 5: Plots showing the clear air speed run data at four altitudes to obtain linear equations for the Water Content Measurement probe (WCM-3000) dry term coefficients. Liquid water content (LWC) element power is plotted on the y-axis and corresponds to the y term in the linear equation. The X term in equation 6 is plotted on the x-axis and corresponds to the x term in the linear equation. Each altitude's parameters including time periods are listed in Table 4. $R^2$ is the coefficient of determination.

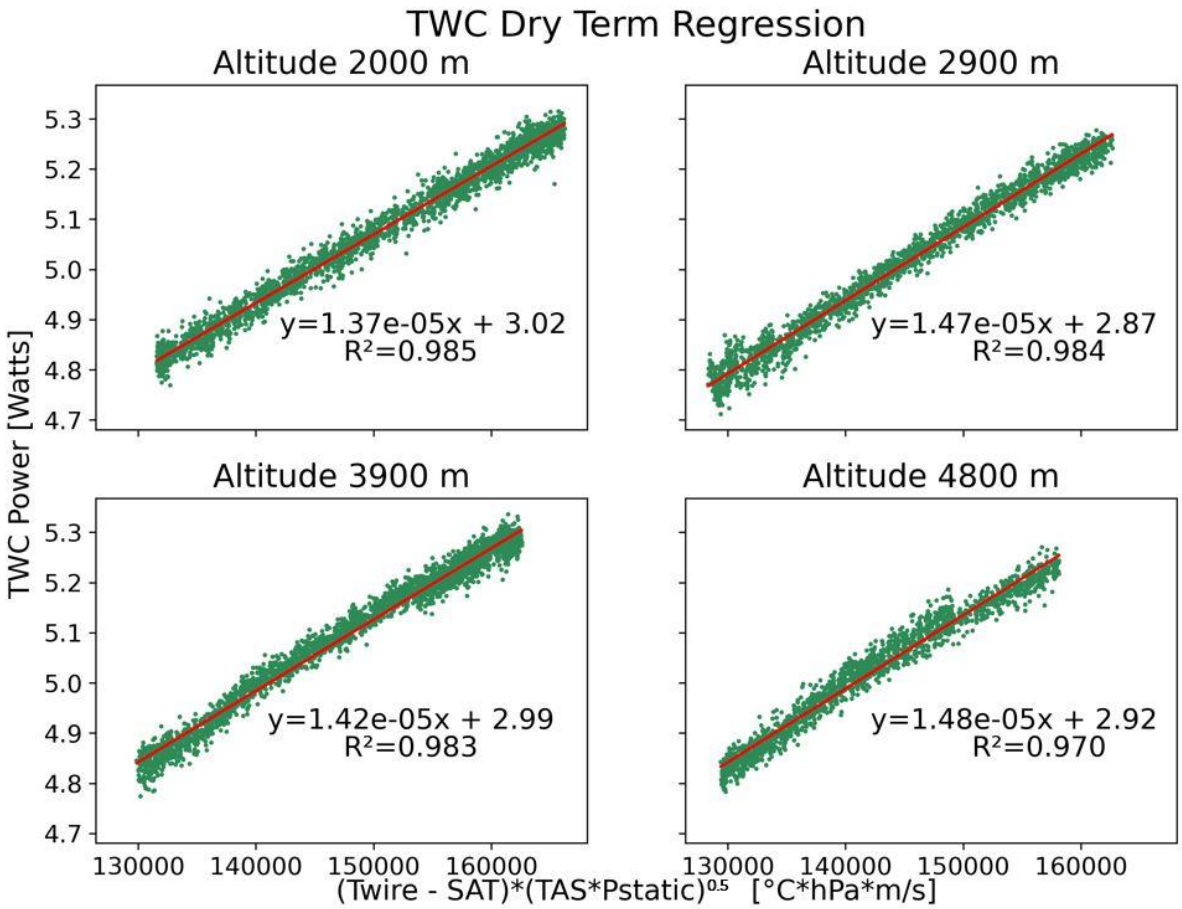


Figure 6: Plots showing the clear air speed run data at four altitudes to obtain linear equations for the Water Content Measurement probe (WCM-3000) dry term coefficients. Total water content (TWC) element power is plotted on the y-axis and corresponds to the y term in the linear equation. The X term in equation 6 is plotted on the x-axis and corresponds to the x term in the linear equation. Each altitude's parameters including time periods are listed in Table 4. $R^2$ is the coefficient of determination.

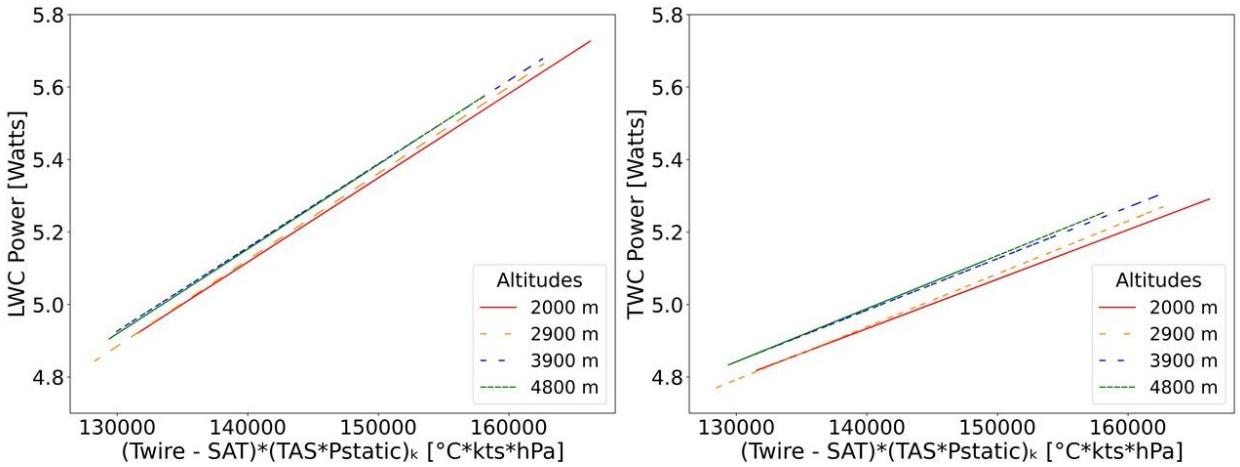


Figure 7: All four lines of best fit calculated for each altitude are plotted for both the Liquid Water Content (LWC – left) and Total Water Content (TWC – right).

*Evaluation of WCM-3000*

Evaluation of the WCM-3000 against LWC measurements from the CDP and King probes is done using data from flight segments corresponding to desired cloud (liquid, SCLW, and mixed phase) environments. To ensure the instruments perform to standard, flight segments are chosen based on cloud droplet diameter ranges as determined from the CDP (<50 µm) and 2D-S (<200 µm) where the WCM-3000, King, and CDP should agree. Note that the CDP cannot measure sizes above 50 µm, so the 2D-S is used to verify droplets up to the size range of the WCM-3000 and King. Since the CDP has the smallest size range, most cases will be analyzed with droplets less than 50 µm. Here, three cloud environments are defined. (1) The liquid water cloud condition represents clouds with liquid water droplets, ideally less than 50 µm, in above freezing temperatures. (2) The SCLW cloud condition represents supercooled liquid water clouds with droplets less than 50 µm. The supercooled liquid water clouds should have little to no ice associated with them. (3) The ice condition is defined as the most complex case in which ice particles are present. The King and CDP do not measure IWC thus making the ice condition more difficult to analyze.

*Liquid Water Cloud Condition*

The liquid water cloud condition focuses on the performance of the WCM in clouds with liquid water droplets less than 50 µm. To obtain cases for this condition, it is important to be flying in clouds that are above freezing and have no sign of ice or supercooled liquid water (SCLW) which are indicative of mixed phase clouds. To determine time periods with liquid water droplets, the aircraft system temperature is first checked to see if the temperature is above 0°C. By plotting temperature and LWC, time periods of above freezing clouds are determined. To ensure no SCLW is present, the RICE probe frequency is examined. A decrease in the RICE probe frequency indicates SCLW. Additionally, to verify there are no ice particles, 2D-S imagery is examined. Since the probes should agree best in clouds with less than 50 µm, the CDP spectrum is used to distinguish if cloud particles diameters peak below 50 µm. Additional spectra from the 2D-S are made to ensure agreement of particle size. Flight segments where altitude and TAS are constant are desired.

*Supercooled Liquid Water Cloud Condition*

The supercooled liquid water cloud condition focuses on the performance of the WCM in clouds with supercooled liquid water droplets less than 50 µm. To obtain cases for this condition, it is important that little to no ice is observed in the SCLW clouds. To determine a time period with SCLW clouds, the RICE probe data are checked for a dampened frequency. 2D-S imagery is examined to ensure no ice is present in the flight segment. The CDP spectrum is used to determine if the cloud droplet diameters are less than 50 µm. Additionally, the temperature should be below 0 °C.

*Mixed Phase Clouds Condition*

The mixed phase cloud condition focuses on the performance of the WCM in clouds with ice particles present. In clouds with ice particles, it is expected that the WCM TWC sensor would measure greater water contents than the WCM LWC sensor. To determine time periods, the WCM

TWC should be greater than the LWC measured. 2D-S imagery is examined to ensure ice particles are present. The 2D-S spectrum is used to determine if ice particle diameters are below 200 μm. There is a total of 3 flight segments examined in this study (Table 5).

Table 5. Table depicts each case type, date, time span, temperature (temp), altitude, mean diameter (diam). The standard deviation from the mean is expressed after ± symbol.

| **Type** | **Date** | **Time Span (hh:mm:ss)** | **Temp.** | **Altitude** | **Diam.** |
|---|---|---|---|---|---|
| LWC | 20221216 | 13:11:38 – 13:12:14 UTC | -0.6 ±0.4 °C | 2864 ±34.6 m | < 50 μm |
| SCLW | 20221212 | 15:10:11 – 15:10:25 UTC | -3.5 ±0.3 °C | 1154 ±3.7 m | < 50 μm |
| Mixed | 20230123 | 14:09:38 – 14:11:30 UTC | -16.8 ±0.2 °C | 5250 ±3.1 m | < 200 μm |

*Uncertainty Calculations*

To determine the absolute error from the WCM, King, and CDP, the measured value is multiplied by the relative error. Each measurement's absolute error is compared. When there is overlap in uncertainties (the absolute error), there is considered to be agreement between the probe's measurements. In (Lilie et al., 2021), the relative error associated with the WCM-3000 measurements is 6%. In (King et al., 1978) the error associated with each measurement is determined as 5% for measurements at 2 g/m$^3$, 8% at 0.5 g/m$^3$, and 16% at 0.2 g/m$^3$. Since the IMPACTS field campaign samples winter storms, most LWC measured by the probes is less than 1 g/m$^3$ with typical King measurements between 0 g/m$^3$ to 1 g/m$^3$. Consistent with these LWC values, a relative error of 10% is used. The CDP has limitations to sizing and counting which affect the calculation of the LWC (Faber et al., 2018). To be consistent each probes uncertainty (absolute error) will be calculated with 10% relative error.

$$Absolute\ Error = Measured\ Value * Relative\ Error \quad (7)$$

# CHAPTER V

# RESULTS

Three cloud conditions (liquid water, SCLW, mixed phase) are defined in chapter 4 to compare the instruments' measured uncertainties. The flight conditions were chosen in environments where (1) the instrument measurements should agree, and/or (2) the environment is typically sampled during the IMPACTS flights. The criteria defined in chapter 4 are used to identify the time segments which are analyzed below.

## Liquid Water Case Analysis

*Environment*

The December 16, 2022 flight observed precipitation over Long Island, NY, with multiple segments sampling warmer than freezing clouds. Outside of takeoff and landing, the longest segment of temperatures above freezing is between 12:47:10 – 13:12:51 UTC (46030 – 47571 seconds from midnight (sfm)) when the P-3 performs a downward spiral over Long Island, NY (Figure 8a). Before 12:47:10 UTC (46030 sfm), the P-3 is flying in clear air allowing for good baseline corrections. The P-3 does its initial downward spiral from 5000 m to 900 m at approximately 12:40 – 12:49 UTC (Figure 8). After transiting at 900 m, an upward spiral is performed until the P-3 reaches 3750 m. At 13:11:42 UTC (47502 sfm), the temperature goes below 0°C and continues to drop the remainder of the assent (Figure 8a). The RICE probe confirms that there is no SCLW present in the clouds sampled during this time segment denoted by the constant frequency (Figure 8b).

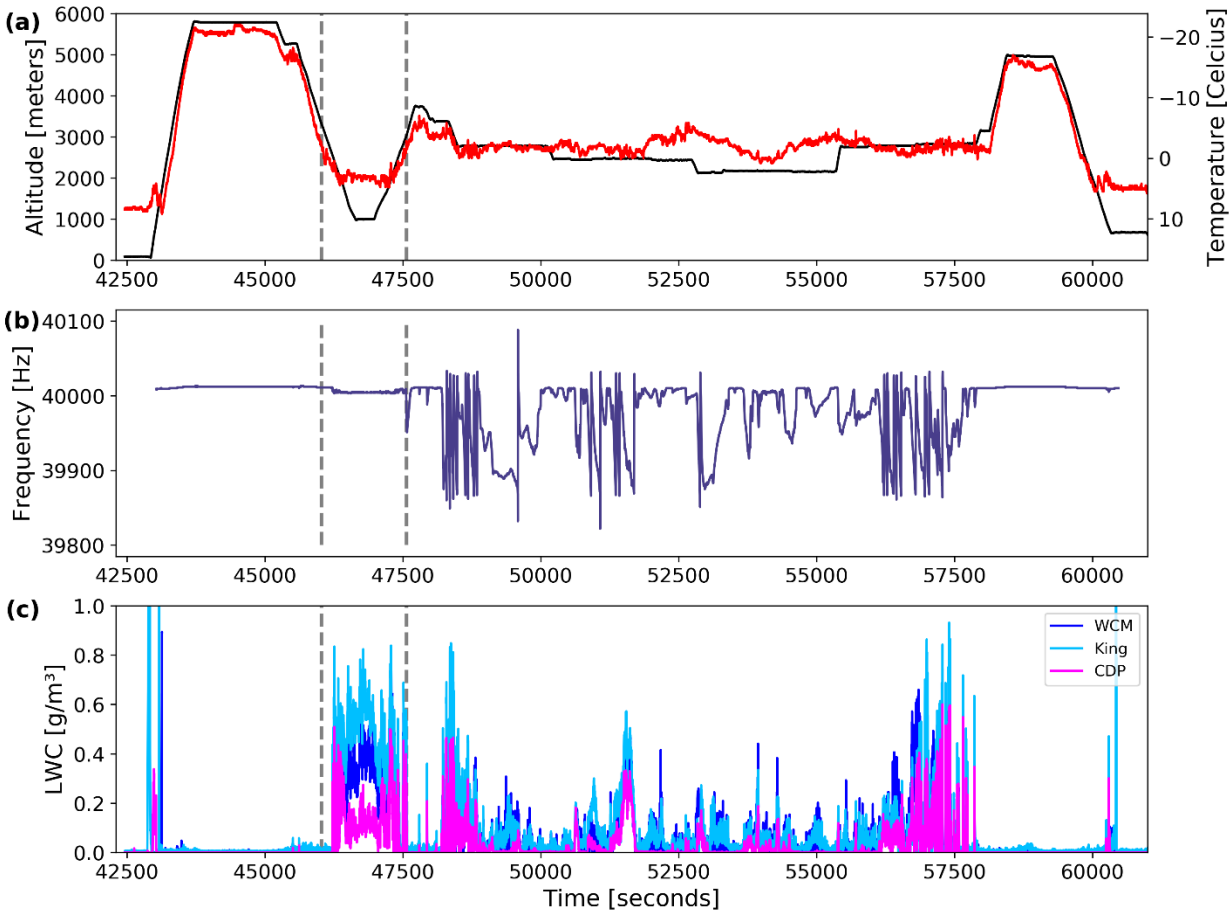


Figure 8: Plots showing the altitude (a – top, black) and air temperature (a – top, red), the Rosemount Icing Detector frequency (b – middle), and liquid water content (c – bottom) on the NASA P-3 Aircraft during the 16 December 2022 flight. The dashed lines denote the start and end of the above freezing analyzed time segment (see Figure 9).

Throughout the 25 minutes, cloud droplets of various sizes are observed (Figure 9). As the P-3 enters cloud at time 12:47:10 UTC (46030 sfm), droplet diameters are less than 50 μm and increase in size as the P-3 continues to descend in cloud. The P-3 is at a constant altitude at times 12:58:20 – 13:03:20 UTC (46700 – 47000 sfm). During this time period large droplets are observed. Even though a constant altitude is preferred for analysis, the large droplet sizes are undesirable. Since it is more imperative to have droplets within range of the instruments, and with the limited amount of data where the P-3 is sampling above freezing clouds, the altitude criterion is ignored for this case. The LWC case analyzed in this study is at time 13:12:36 – 13:13:16 UTC

(47556 – 47596 sfm) where there is an in and out of cloud penetration. The CDP spectrum (Figure 10) shows a large concentration of droplets below 50 µm during this time period. There is a slight increase in droplets in the CDP spectrum at 50 µm, raising the concern that there may be droplets larger than the CDP size range. The 2D-S spectrum (Figure 11) is measuring droplet diameters below 200 µm, which is in the size range for the King and WCM. Since the largest concentration of droplets is below 50 µm, and there are limited data for this condition, the criterion of droplets less than 50 µm is relaxed to small droplets.

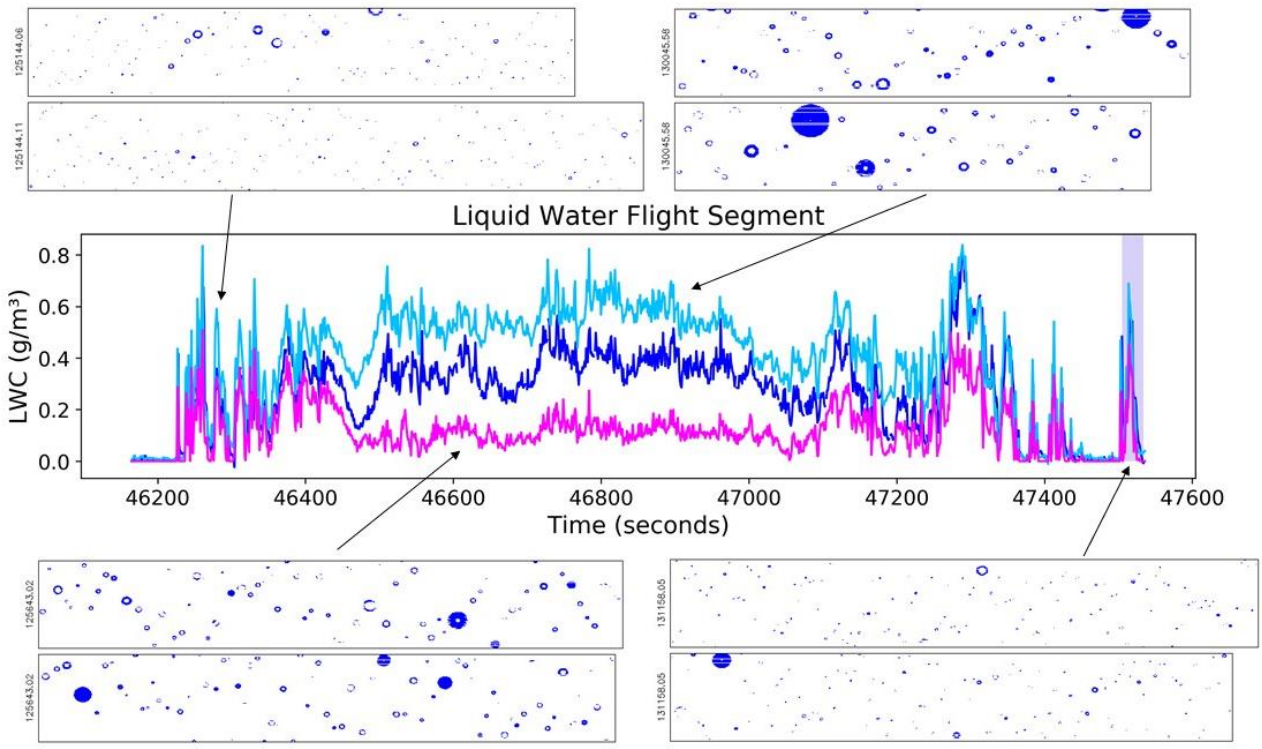


Figure 9: Time series of liquid water contents for the King (light blue), WCM (dark blue), and CDP (magenta) during the 25-minutes where the P-3 is flying in above freezing liquid water clouds on 16 December 2022. 2D-S images are overlaid with arrows pointing to respective time. The purple highlighted region is the analyzed liquid water flight segment (see Figure 12).

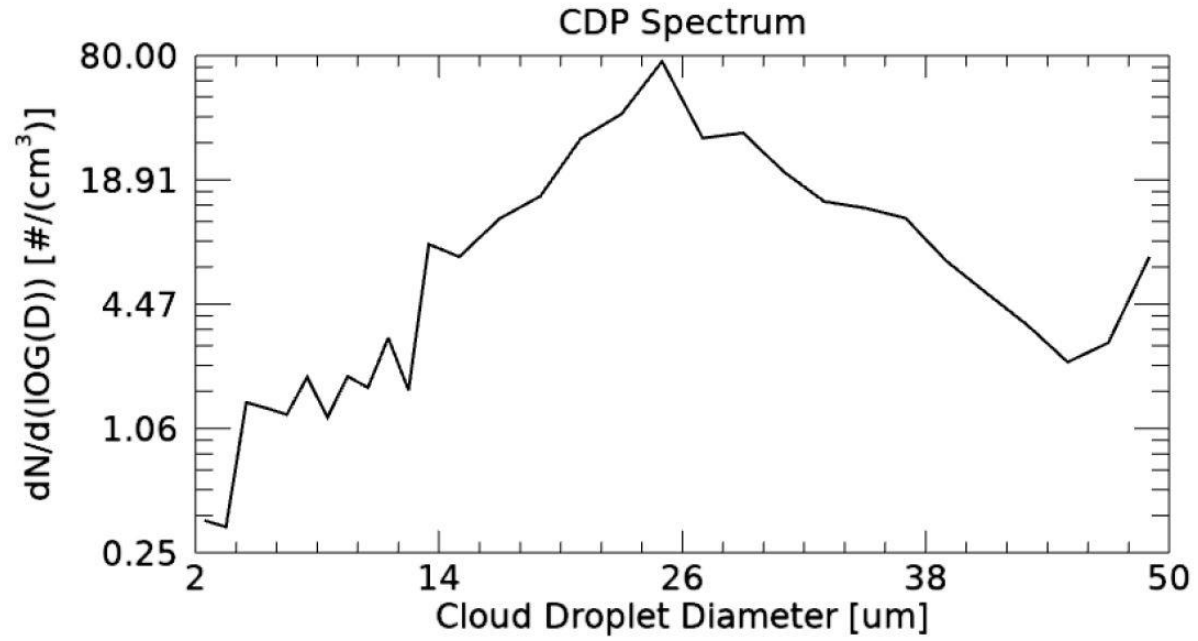


Figure 10: Size distribution of particles measured from the Cloud Droplet Probe for liquid water flight segment at times 13:11:38 – 13:12:14 UTC (47498 – 47534 seconds from midnight) (see Figure 12).

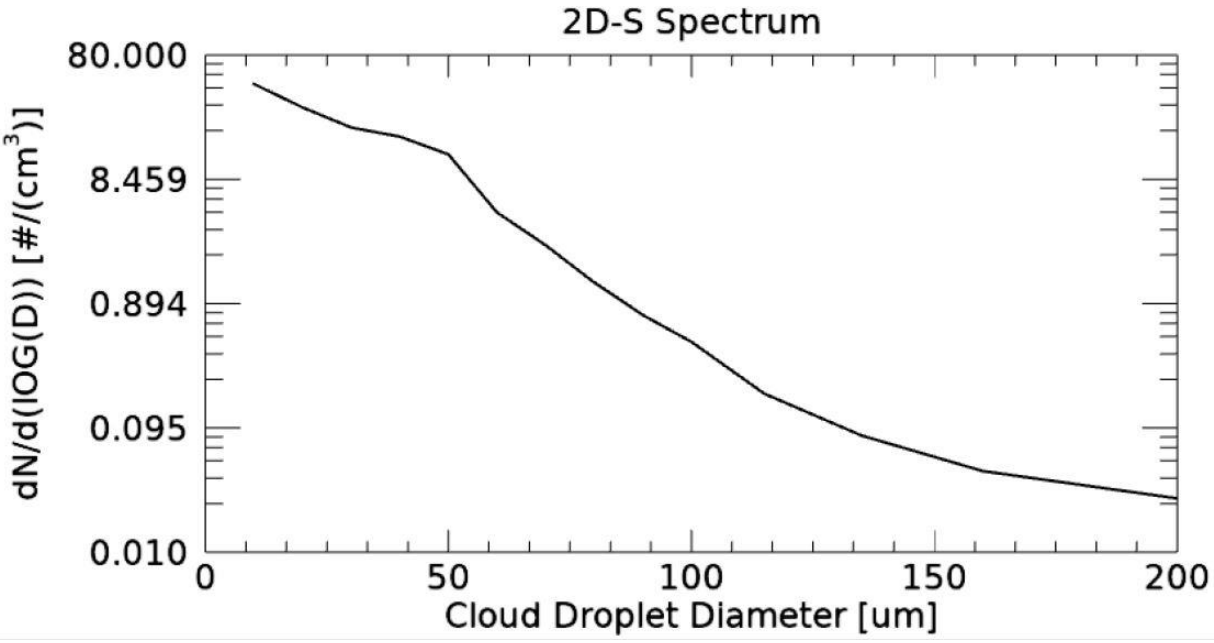


Figure 11: Size distribution of particles measured from the 2D-S during the liquid water flight segment at times 13:11:38 – 13:12:14 UTC (47498 – 47534 seconds from midnight) (see Figure 12).

A time series of LWC with associated uncertainties measured from the WCM, King, and CDP for the liquid water case is plotted in Figure 12. There is general correlation in the trend of measured LWC but very little overlap in the uncertainty of each measurement. In the cloud pass, the probes measure a gradual increase in LWC until peak LWC values are reached. During this time, some uncertainties are overlapping. The King reaches its peak LWC value at 0.69 $g/m^3$ at time 13:11:53 UTC (47513 sfm). The WCM and CDP reach their peak LWC at time 13:11:54 UTC (47514 sfm), where the WCM measures 0.57 $g/m^3$ and the CDP measures 0.45 $g/m^3$. An overlap in the WCM and King uncertainty is seen when the WCM reaches its first peak LWC value. The WCM and King continue to have overlapped uncertainties until the WCM measures a second peak in LWC at time 13:11:58 UTC (47518 sfm), where the King and CDP begin to show a decrease in LWC. At time 13:12:05 UTC (47525 sfm), the CDP measures no LWC, meaning the P-3 is out of cloud. The WCM decreases in LWC until time 13:12:12 UTC (47532 sfm) where no LWC is measured.

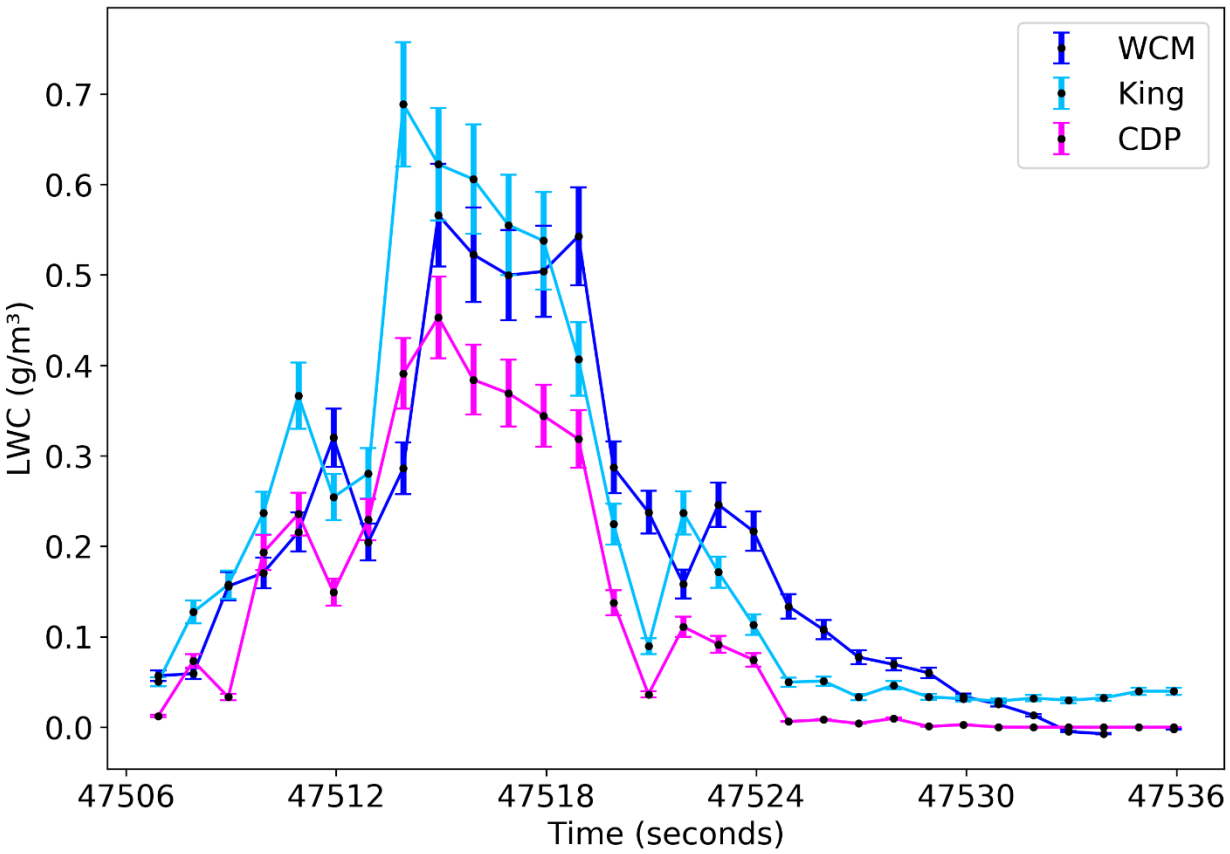


Figure 12: Time series of 1 Hz liquid water content (LWC) for the above freezing liquid water clouds on 16 December 2022. Each point has an uncertainty of 10% represented by the error bars.

## Supercooled Liquid Water Case Analysis

*Environment*

A flight on 12 December 2022 observed stratocumulus clouds off the shore of New Jersey with both in cloud and clear air segments. The desired segment of this flight is the stratocumulus clouds sampled at 11 km with temperatures at -3 °C (see Figure 13a). The P-3 was flying in and out of cloud during this time period sampling SCLW with cloud droplet diameters less than 50 µm being fairly uniform in each cloud. The P-3 did a few speed run maneuvers in cloud while flying through stratocumulus clouds (Figure 14). At time 15:10:00 – 15:12:50 UTC (54600 – 54770 sfm) the TAS is 105 $ms^{-1}$. The P-3 increased its speed to 130 $ms^{-1}$ and stayed at that TAS until 15:17:56 UTC (55076 sfm). The P-3 increased its TAS again to 150 $ms^{-1}$ until 15:21:25 UTC (55285 sfm). Even

though there were speed run maneuvers occurring during this stratocumulus segment, the TAS was constant over the case examined for the SCLW condition allowing for this flight to be ideal for comparing LWC amounts for the probes in supercooled conditions.

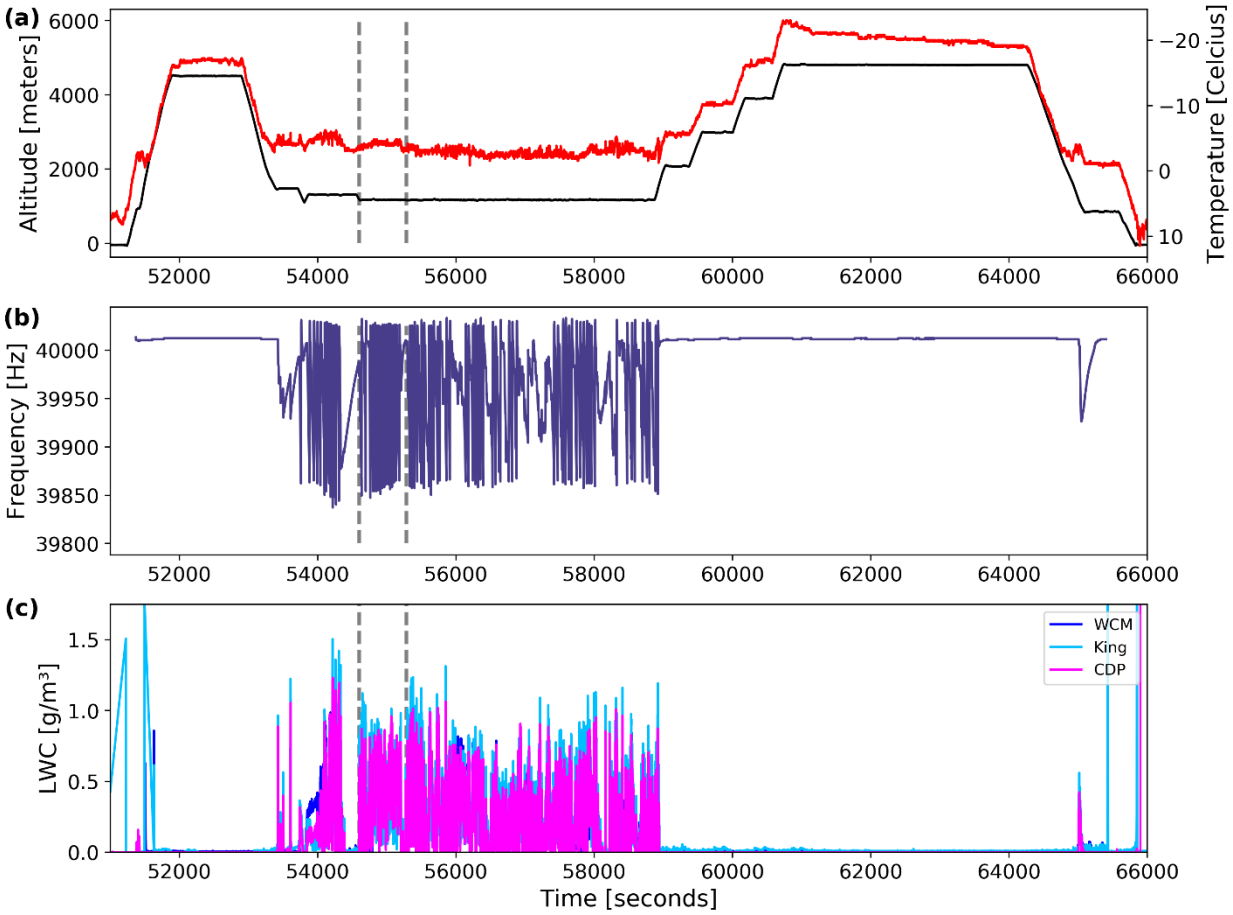


Figure 13: Plot showing the altitude (a – top, black) and air temperature (a – top, red), the Rosemount Icing Detector frequency (b – middle), and liquid water content (c – bottom) on the NASA P-3 Aircraft during the 12 December 2022 flight. The dashed lines denote the desired time segment (see Figure 15) where the P-3 samples stratocumulus clouds with supercooled liquid water.

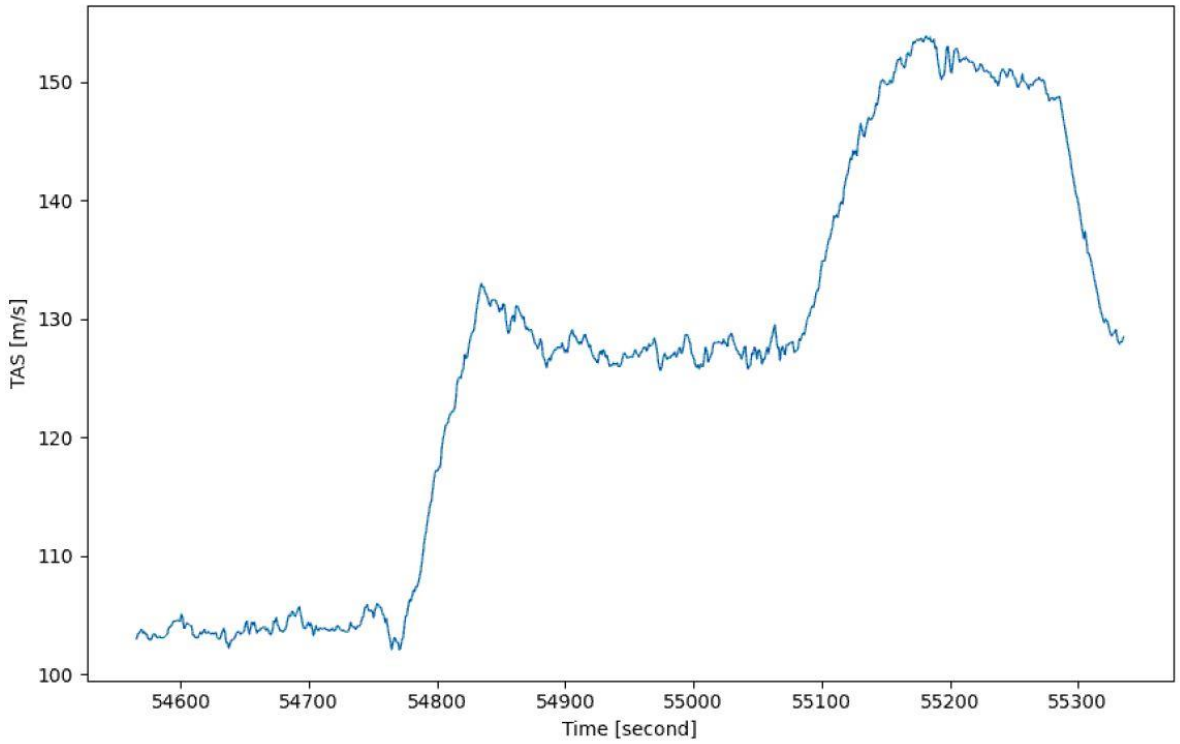


Figure 14: True airspeed (TAS) maneuvers during the period of stratocumulus clouds at times 15:08:46 – 15:22:53 UTC (54526 – 55373 seconds from midnight).

A 12-minute segment where LWC is sampled in a region of stratocumulus clouds is plotted in Figure 15 with 2D-S images overlaid with arrows pointing to the sampled time. At the beginning of the segment, the P-3 flew through intermittent cloud passes. The P-3 eventually entered cloud and stayed in cloud until 15:20:00 UTC (55200 sfm) preceded by clear air with occasional smaller cloud passes. Since the flight segment has fairly uniform conditions (i.e. droplets less than 50 µm, constant temperature and altitude), one cloud pass is chosen to study. The SCLW case is at time 15:10:07 – 15:10:25 UTC (54607 – 54625 sfm) (Figure 17). During this cloud pass, cloud droplet diameters are < 50 µm (Figure 16). Since the cloud droplets are < 50 µm in uniform conditions it is expected that the instruments would measure the same LWC amounts.

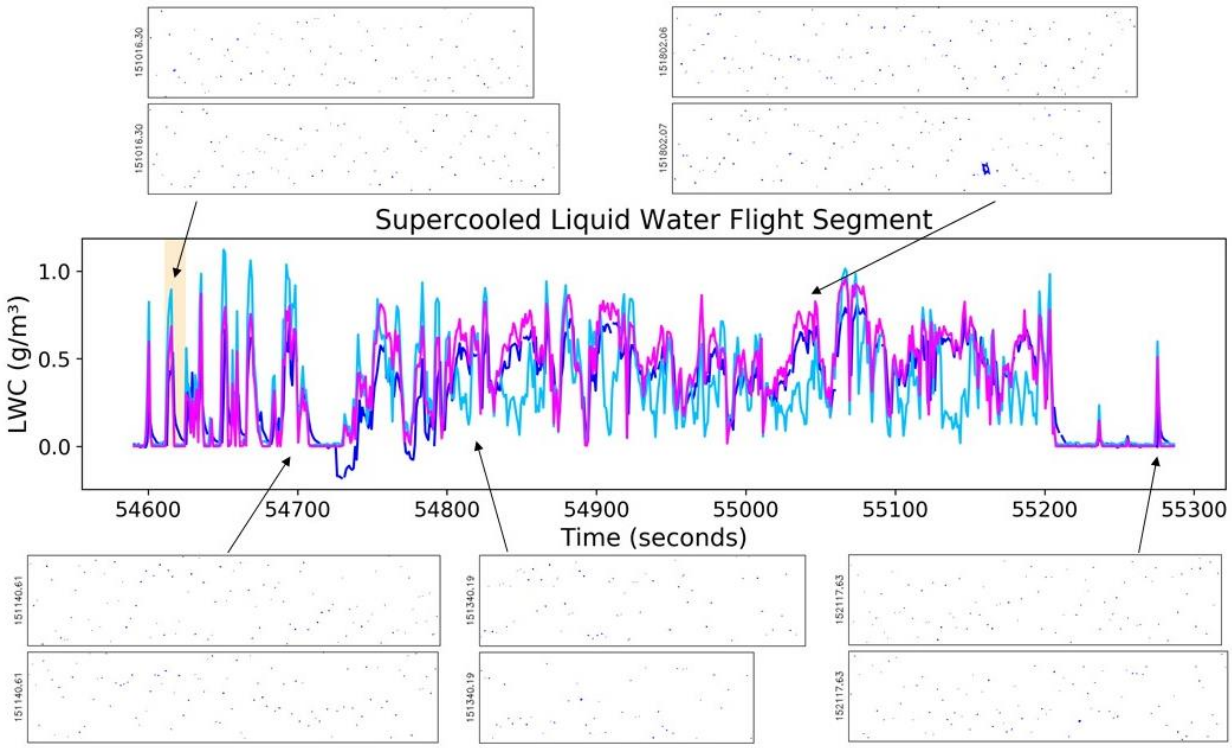


Figure 15: Plot showing liquid water contents for the King (light blue), WCM (dark blue), and CDP (magenta) for the supercooled liquid water flight segment on 12 December 2022. 2D-S images are overlaid with arrows pointing to respective time. The yellow highlighted region is the analyzed supercooled liquid water flight segment (see Figure 17).

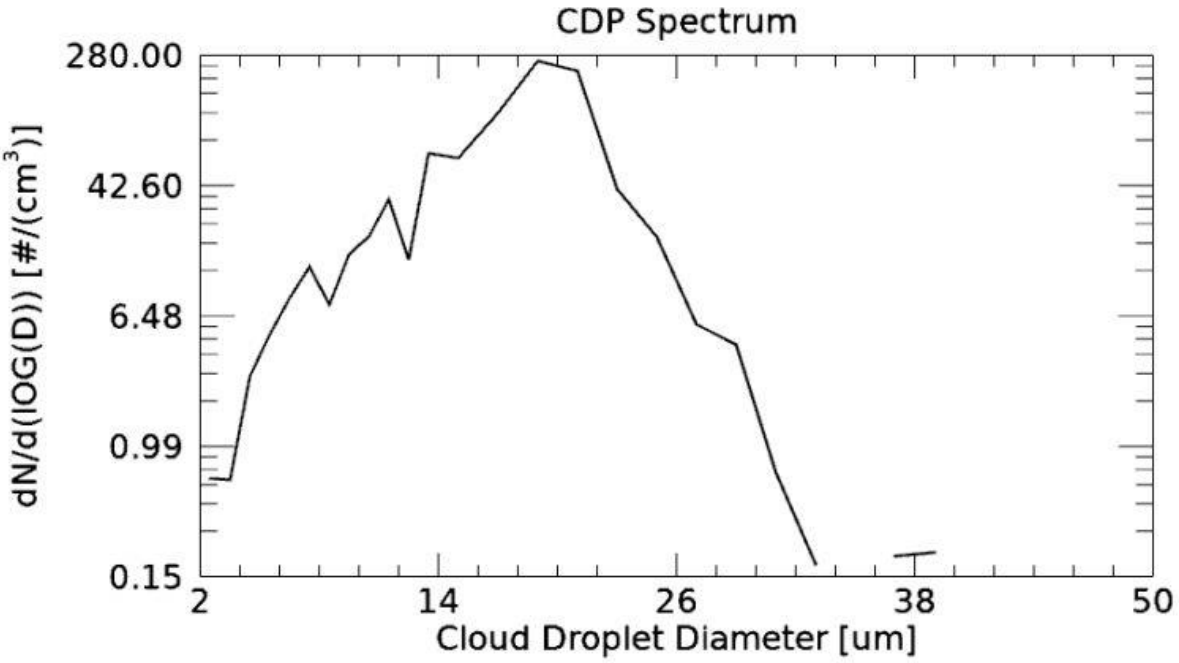


Figure 16: Cloud Droplet Probe (CDP) droplet size distributions for the supercooled liquid water (SCLW) on 12 December 2022 at times 15:10:11 – 15:10:25 UTC (54611 – 54625 seconds from midnight) (see Figure 13).

A time series of LWC with associated uncertainties from the WCM, King, and CDP for the SCLW case is plotted in Figure 17. General agreement in the trend of LWC is seen by the instruments measuring the same increase and decrease in LWC. However, there is no agreement in the measured LWC denoted by no overlapping uncertainties during the increase and peak LWC's measured. The WCM begins to measure LWC one second after the King and CDP. The King is 0.2 g/m$^3$ greater than the CDP and the CDP is 0.2 g/m$^3$ greater than the WCM at the peak. Both the King and CDP measure zero LWC at time 15:10:18 UTC (54618 sfm), while the WCM measures 0.2 g/m$^3$. The King and CDP measure no LWC for the remaining 7 seconds. The WCM LWC gradually tapers off until reaching close to zero g/m$^3$ at time 15:10:25 UTC (54625 sfm).

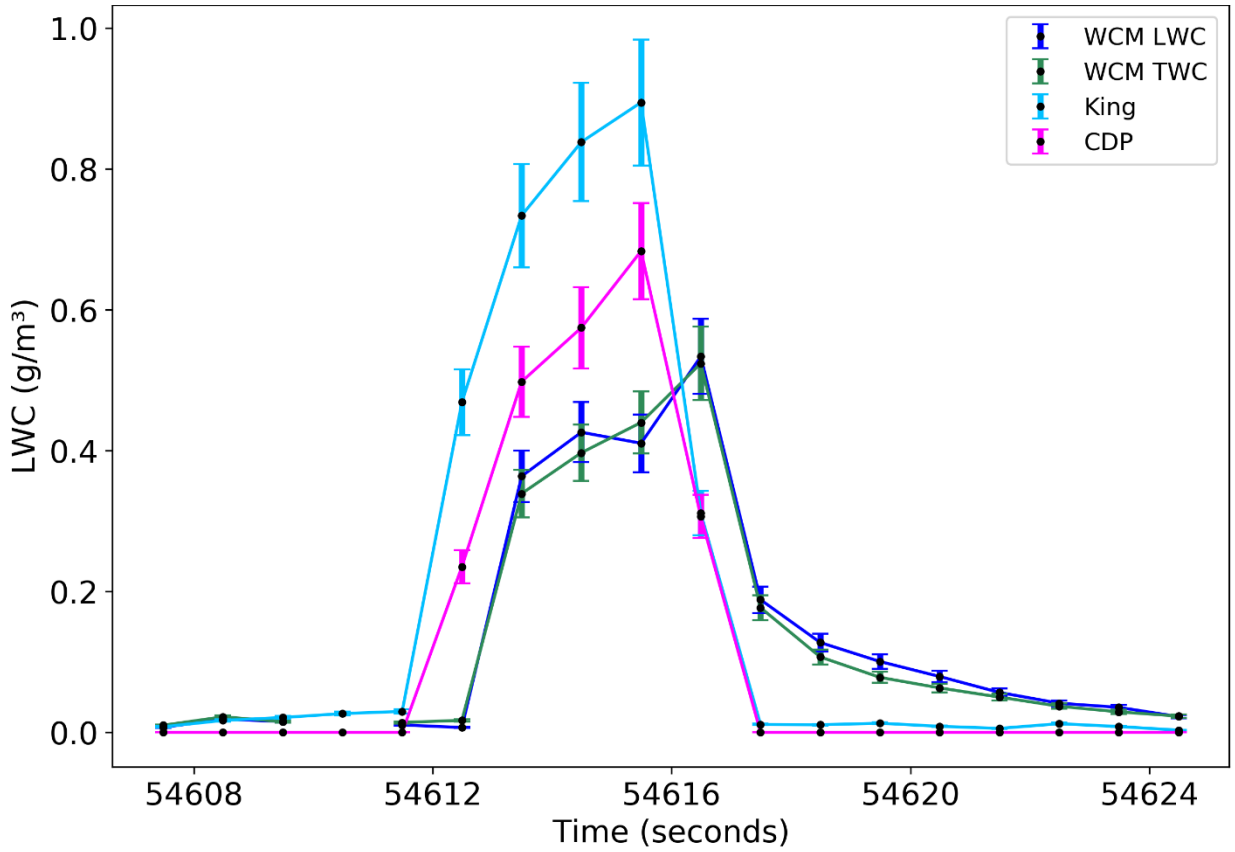


Figure 17: Time series of 1 Hz liquid water content (LWC) for the supercooled liquid water (SCLW) stratocumulus clouds on 12 December 2022. The uncertainty at each point is 10% represented by the error bars.

## Mixed/Ice Phase Case Analysis

*Environment*

The 23 January 2023 science flight sampled a winter storm system affecting the New England and Gulf of Maine region. Other than at take-off, the air temperature stayed below zero for the entire flight (Figure 18a). The time period chosen for analysis is during a section of a flight leg where the P-3 sampled mixed phase clouds at 5 km. During this time intermittent periods of SCLW is sampled, denoted by the dampened RICE frequency (see Figure 18b). Rimed ice particles, sideplanes, and irregular aggregates were also sampled during the desired time period (see Figure 19). The WCM TWC values indicated the largest amount of water content during this time period.

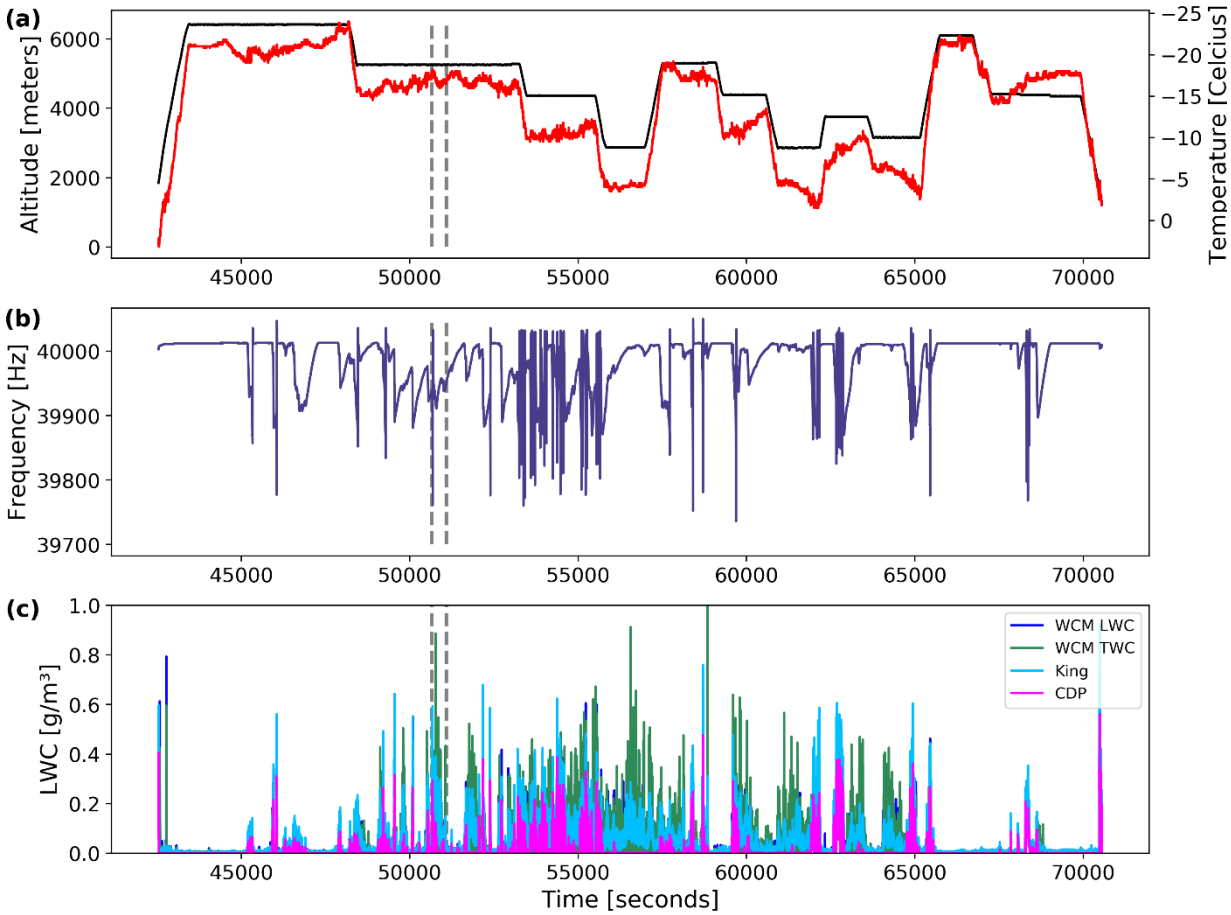


Figure 18: Plots showing the altitude (a – top, black) and air temperature (a – top, red), the Rosemount Icing Detector frequency (b – middle), and liquid water content (c – bottom) on the NASA P-3 Aircraft during the 23 January 2023 flight. The dashed lines denote the time segment (Figure 21) where the P-3 samples mixed phase clouds.

A 7-minute segment where both LWC and TWC is sampled in mixed phase clouds is plotted in Figure 19 with 2D-S images overlaid with arrows pointing to the sample time. The P-3 flew in clouds during the whole 7-minute segment until it exits cloud at the very end of the time period. The 2D-S images show periods of SCLW, rimed aggregates, sideplanes, and other ice particles. The case chosen to study is at time 14:09:38 – 14:11:30 UTC (50978 – 51090 sfm) where mostly ice particles are being sampled. The time period is chosen since it is at the very edge of the cloud, to see if the WCM TWC and LWC elements have a similar trend in the decrease in water content after exiting cloud as seen in the other cases. During this time period,

there are cloud droplet diameters less than 200 µm (Figure 20). While it is not a large concentration of particles present, the particle diameters are within range for the WCM.

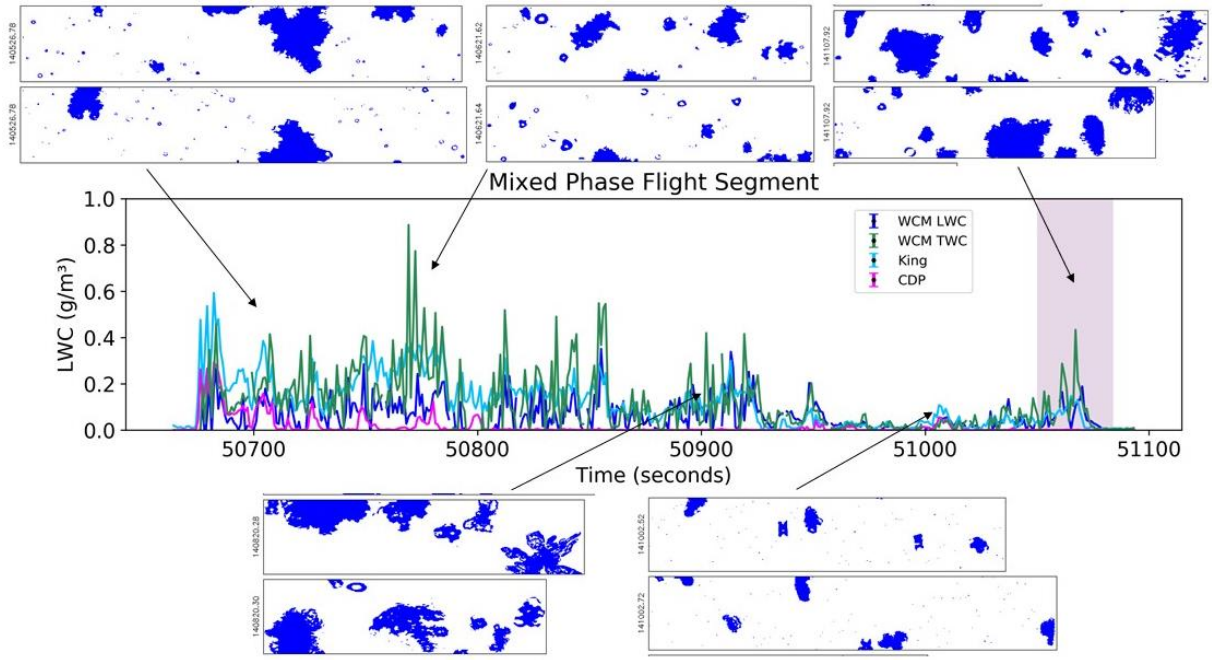


Figure 19: Time series of liquid water contents for the King (light blue), WCM LWC (blue), WCM TWC (green), and CDP (magenta) for the ice/mixed phase cloud flight segment on 23 January 2023. The purple highlighted region is the analyzed mixed phase cloud flight segment (see Figure 21).

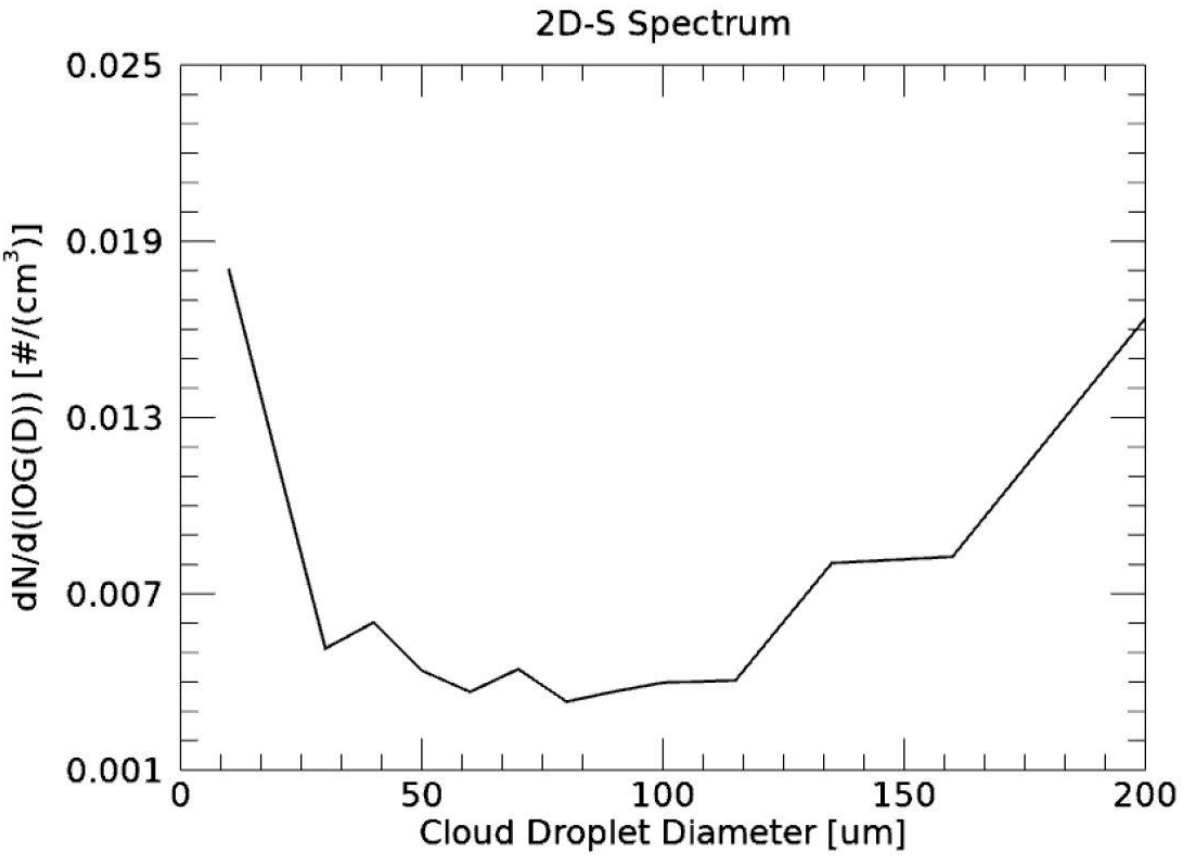


Figure 20: 2D-S droplet size distributions from the mixed phase cloud case on 23 January 2023 at times 14:09:38 – 14:11:30 UTC (50978 – 51090 seconds from midnight) (Figure 21).

A time series of LWC and TWC with associated uncertainties is plotted in Figure 21. There is some small agreement between the WCM LWC and King. Overall, the WCM TWC is reporting the largest water contents. The CDP shows no LWC throughout the whole time period. 2D-S images show a variety of particle types including droplets and rimed aggregates (Figure 19). The particle types and diameters are out of range of the CDP therefore no LWC is measured. The largest LWC measured during this time period is 0.2 g/m$^3$ from the WCM. The largest peak TWC is at time 14:11:07 UTC (51067 sfm). At the very end of the time period the instruments measure no water contents. According to the 2D-S particle concentrations (Figure 22) over this time period the P-3 exits cloud at 14:11:16 UTC (51076 sfm). The WCM LWC appears to have a slower response to exiting cloud since it gradually tapers off to zero.

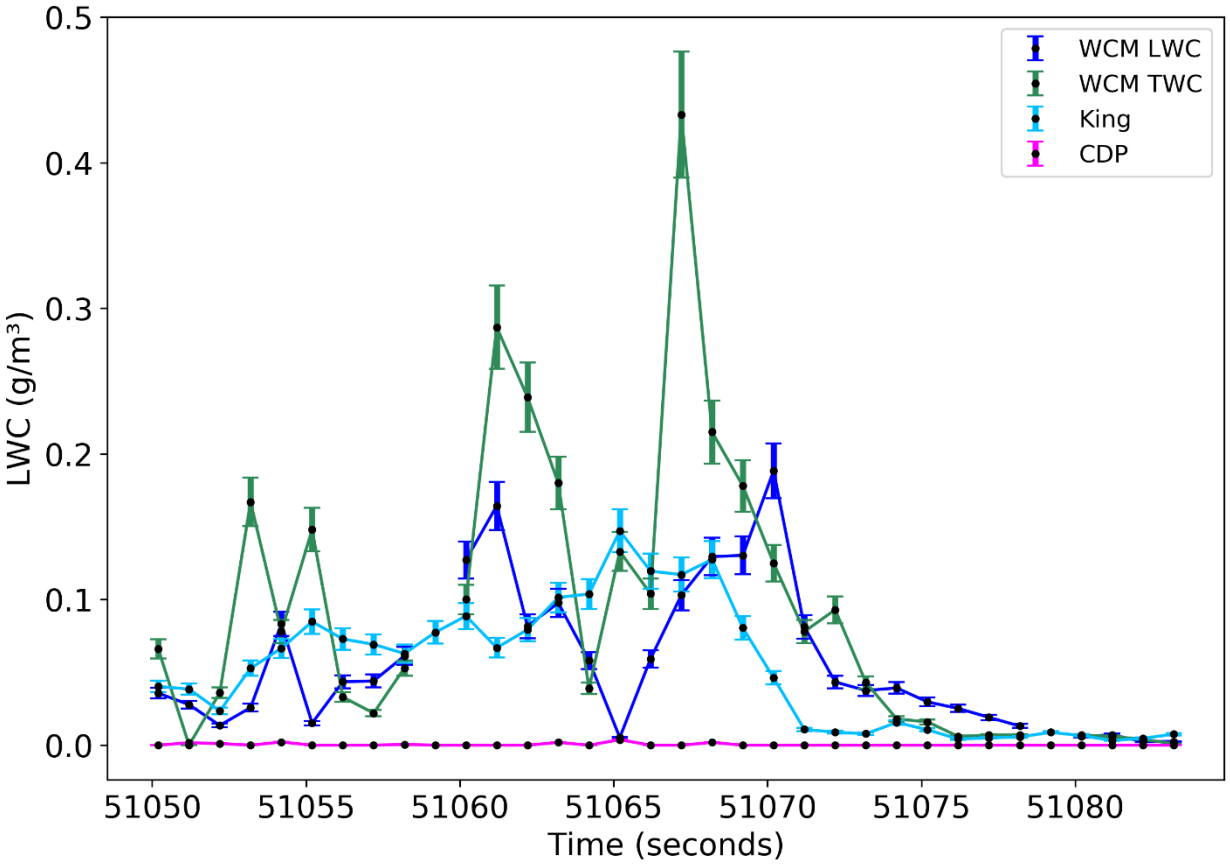


Figure 21: Time series of 1 Hz liquid water content (LWC) and total water content (TWC) data in mixed phase clouds on 23 January 2023. The uncertainty at each point is 10% represented by the error bars.

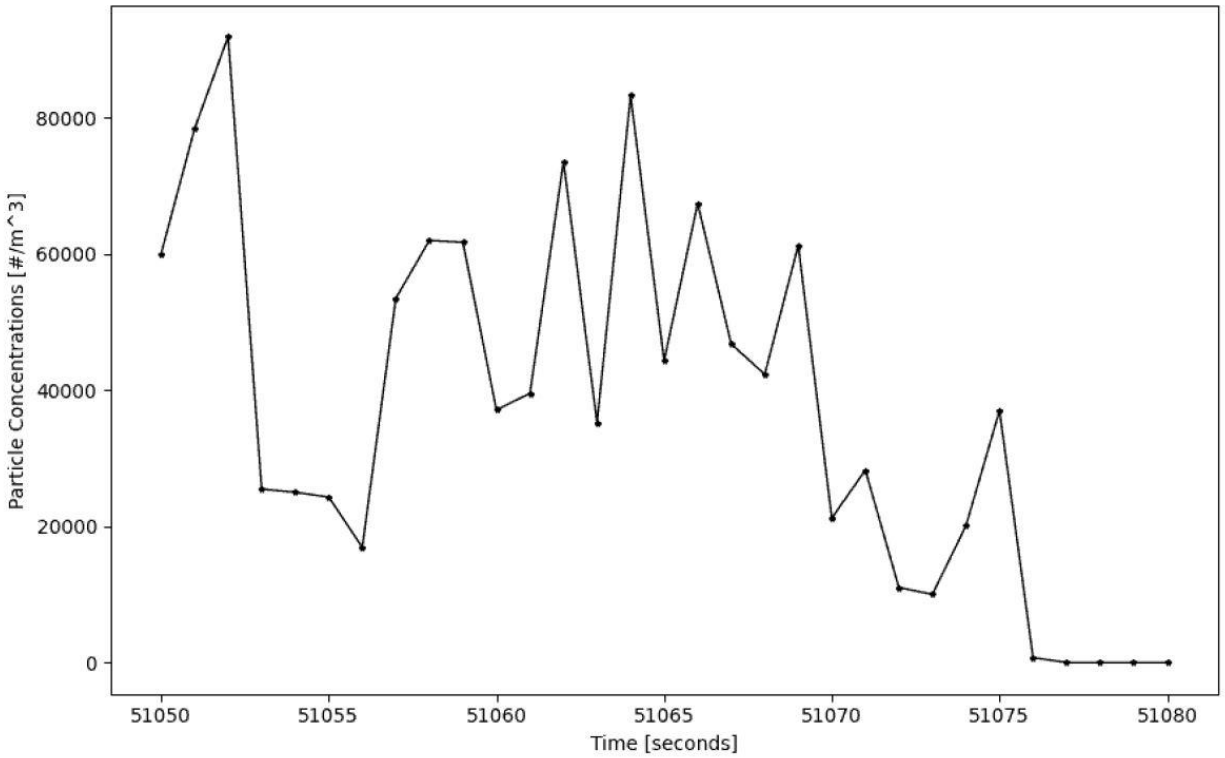


Figure 22: 2D-S vertical channel total normalized particle concentrations for all bin sizes from the mixed phase cloud case on 23 January 2023 at times 14:09:38 – 14:11:30 UTC (50978 – 51090 seconds from midnight) (Figure 21).

# CHAPTER VI

# DISCUSSION

In the liquid water case, the King is measuring the greatest amount of LWC between the three probes. A lower CDP LWC could be due to two things; (1) some of the droplets observed during the time period are outside the CDP measurement size range, (2) the CDP may have incorrect size bins. Bead tests for the CDP are applied to fix any underrepresentation of droplet sizes. Slight variations in channel sizes can affect the calculated LWC. The WCM also reported lower LWC values than the King during this case. While it can be difficult tell, there is a shift in the measurements by one second compared to the King. Any variation in LWC measured by the WCM happens one second after the King and CDP. Additionally, the WCM has a slow decline in LWC once the P-3 is out of cloud. Overall, the WCM and King did not always agree within their measured uncertainty during this time period.

In the SCLW case, the King reported the greatest amount of LWC. The CDP indicated less LWC compared to the King, but values are greater than the WCM. The spectrums from the CDP show the droplets are within range of all three instruments, yet the instruments do not agree within their measured uncertainties. A likely cause of the lower CDP LWC is due to not having the field project's quality control data not being applied to adjust the channel sizes from their default values. The default channel sizes are likely too small, which reduces the calculate LWC. Similar to the liquid water case, the WCM begins measuring LWC one second after the King and CDP. It is very prominent in this case that the WCM is measuring half the amount of LWC than the King. For the WCM to agree with the King, it would need an uncertainty of 100%.

In the mixed phase case, it was expected that there would be little agreement since the King and CDP do not measure ice. As expected, the CDP measured no LWC during this time period.

Ice particles that pass through the CDP's optical field are not measured since the scattered light is not between 4 – 12°. The King and WCM both measure around 0.05 g/m$^3$ occasionally reaching 0.2 g/m$^3$ of LWC. While this is a mixed phase cloud, this specific case mostly consisted of ice particles. Hot-wires are susceptible to measuring some ice when the particle comes directly in contact with the wire, but it is expected that it would be a residual amount. The WCM TWC element was measuring the most amount of water contents at this time, which is expected. Since there was no other instrument used in this study to measure TWC there is no comparison for the WCM TWC. The main takeaway in this case is the slow decline seen in both the TWC and LWC measurements from the WCM once out of cloud. Since the liquid water and SCLW cases show this decline once out of cloud, it was important to verify that the mixed phase case also sees this same decline.

Throughout the cases analyzed, little agreement between the probes is observed. The WCM performance could be a result of a time offset, a hysteresis effect, a software issue, or an overdamped control system. A time offset would be seen as a simple shift in time. The WCM data would follow a similar trend to the King and CDP, but the time of measurement would be off by a second. Since the WCM performance has the gradual decline in LWC and not just a simple shift in the time of measurement, this is likely not the cause. Another idea posed is that the WCM is experiencing a hysteresis effect due to liquid water not evaporating off the wire. Initially, the insulating spacer between the sensor element and the strut of the WCM was considered a place where water could easily be trapped. After some lab testing and discussions with the SEA manufacturer, this is likely not the cause. A software issue was discussed with SEA as the potential cause of this performance issue. The M300 data acquisition system used to run and collect the WCM measurements had an older version of the WCM software. This software was not collecting

the data at the typical update rate, averaging the data over 16 seconds instead of 8 seconds. After updating the software, the performance is still the same. Additionally, the performance did not change with a new sensor head. This performance issue is seen in the raw data, not just the calculated LWC. Therefore, this is likely an issue with the measurement not the calculation. An overdamped control system is based on the response of the control system to a change in the environment. As liquid water comes in contact with the sensor, the input to the control system signals the probe to supply more power. Once more power is supplied, the liquid water evaporates. In an overdamped system, the control system is not supplying enough power initially to evaporate all the liquid water. Less liquid water is evaporated initially, causing the lower peak in LWC seen in the cases. The remaining amount of water takes longer to evaporate resulting in the slow decline in LWC seen in the WCM measurements.

To better understand the time response of the WCM a time constant ($\tau$) is computed. The time constant (Duchon & Hale, 2012) refers to the exponential decay related to the time it takes for the WCM to measure zero LWC once out of cloud. One of the major reasons to compute the time constant is to see if there is consistency in the time it takes for the WCM to evaporate the remaining liquid water once out of cloud, particularly for the cases analyzed. Figure 28 helps explain how to compute the time constant. $LWC_o$ is the initial LWC measured when the WCM is out of cloud. $LWC_s$ is 37% of $LWC_o$, or 1 step change in LWC. To compute $\tau$, equation 8 is rearranged. The out of cloud time is found using the CDP or the 2D-S, depending on the case. Once the CDP/2D-S measure no LWC/particles the P-3 is considered to be out of cloud. $LWC_s$ is found by multiply $LWC_o$ by 37%, and the closest measured value from the WCM to the calculated $LWC_s$ is used. The time (t) is found by counting from $LWC_o$ to $LWC_s$.

$$\frac{LWC_s - LWC_\infty}{LWC_0 - LWC_\infty} = e^{-t/\tau} \quad (8)$$

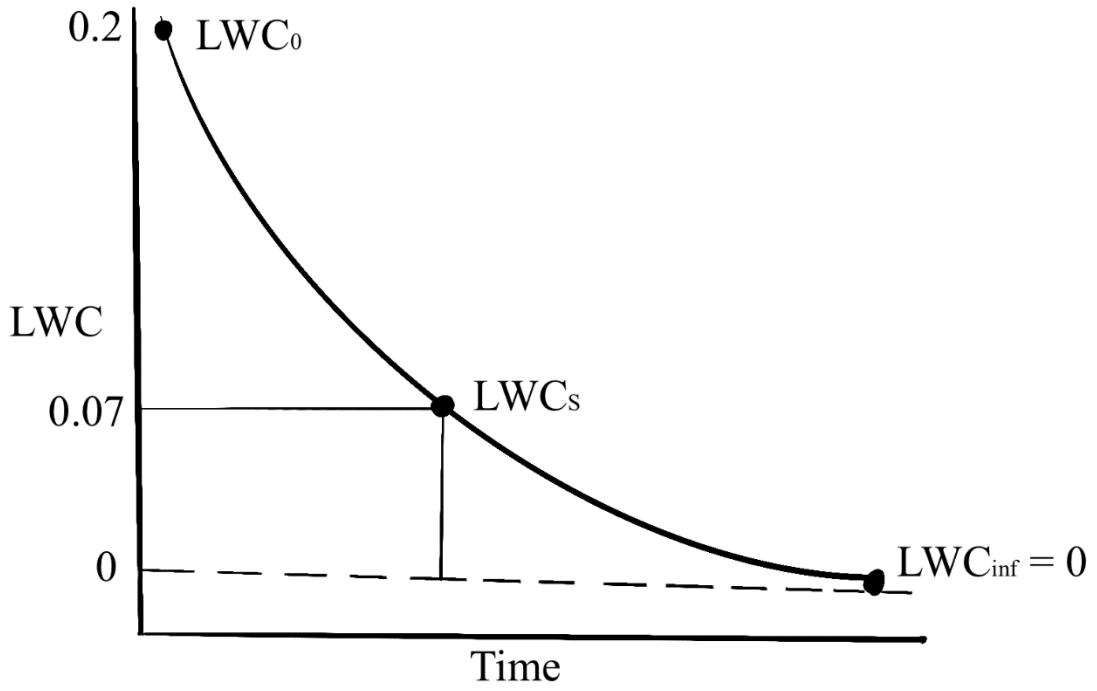


Figure 23: Image showing time constant concept. The concept is applied to determine the time it takes for the liquid water content (LWC) to reach 0 g/m$^3$, where $LWC_o$ is the initial time once the WCM is out of cloud. $LWC_s$ is 37% of the $LWC_o$, which is one step change in LWC.

Tau is computed for the WCM LWC for each case in each flight segment type; i.e. LWC, SCLW, and Ice. In the liquid water case, $\tau$ = 3.4 s. In the SCLW case, $\tau$ = 3.4 s. In the mixed phase case, $\tau$ = 3.6 s for the WCM LWC, and $\tau$ = 2.9 s for the WCM TWC. The time constant was calculated for additional time periods and found to overall be $\tau \sim 3$ s.

# CHAPTER VII

# CONCLUSION

By analyzing three cloud conditions during the NASA IMPACTS field project, this research has shown that the WCM-3000 does not agree with the King and CDP within their measured uncertainties. In the liquid water condition the probes did not agree due to larger droplets being present. In the SCLW cloud condition, the probes are expected to agree, but the King probe is measuring much larger LWC than the WCM and CDP. In all three cases, the WCM has a slow decline in LWC once out of cloud alluding to an overdamped control system, which has a time constant of ~ 3 seconds. Future research is needed to confirm the cause of the WCM-3000 performance issues. Once the cause is confirmed, it may be possible to correct for this issue using a post-processing algorithm. It is suggested that IMPACTS 2022 and 2023 data users use the King probe measurements for LWC. The uncertainty of the WCM total and liquid water content can be up to 100%.

# AVAILABILITY

The IMPACTS cloud microphysics probes dataset was used for this study. The ADPAA (Delene, 2011) software was used to process the data. The WCM-3000 processing module is a part of ADPAA. The wcm3000tocorrect.py script is used to calculate the adjusted TWC and LWC for the Water Content Measurement (WCM-3000) probe, and has been added to ADPAA. The wcm3000_calib.py script is used to calculate the clear air speed run calibration, and has been added to ADPAA. A guide to aircraft quality assurance is given in appendix A. Plots in this study were made using modules in python with matplotlib (Hunter, 2007).

## REFERENCES


Brown, P. R. A., & Francis, P. N. (1995). Improved Measurements of the Ice Water Content in Cirrus Using a Total-Water Probe. *Journal of Atmospheric and Oceanic Technology*, *12*(2), 410–414. https://doi.org/10.1175/1520-0426(1995)012<0410:IMOTIW>2.0.CO;2

Claffey, K. J., Jones, K. F., & Ryerson, C. C. (1995). Use and calibration of Rosemount ice detectors for meteorological research. *Atmospheric Research*, *36*(3), 277–286. https://doi.org/10.1016/0169-8095(94)00042-C

David Delene, M. R. P. (2020). *UND Cloud Microphysics IMPACTS* [dataset]. NASA Global Hydrometeorology Resource Center Distributed Active Archive Center. https://doi.org/10.5067/IMPACTS/MULTIPLE/DATA101

Delene, D. J. (2011). Airborne data processing and analysis software package. *Earth Science Informatics*, *4*(1), 29–44. https://doi.org/10.1007/s12145-010-0061-4

Duchon, C., & Hale, R. (2012). *Time Series Analysis in Meterology and Climatology: An Introduction*. Wiley-Blackwell.

Dye, J. E., & Baumgardner, D. (1984). Evaluation of the Forward Scattering Spectrometer Probe. Part I: Electronic and Optical Studies. *Journal of Atmospheric and Oceanic Technology*, *1*(4), 329–344. https://doi.org/10.1175/1520-0426(1984)001<0329:EOTFSS>2.0.CO;2

Faber, S., French, J. R., & Jackson, R. (2018). *Laboratory and In-flight Evaluation of a Cloud Droplet Probe (CDP)*. https://doi.org/10.5194/amt-2017-479

Hunter, J. D. (2007). Matplotlib: A 2D Graphics Environment. *Computing in Science & Engineering*, *9*(3), 90–95. https://doi.org/10.1109/MCSE.2007.55

King, W. D., Parkin, D. A., & Handsworth, R. J. (1978). A Hot-Wire Liquid Water Device Having Fully Calculable Response Characteristics. *Journal of Applied Meteorology*, *17*(12), 1809–1813. https://doi.org/10.1175/1520-0450(1978)017<1809:AHWLWD>2.0.CO;2

Korolev, A., & Isaac, G. (2003). Phase transformation of mixed-phase clouds. *Quarterly Journal of the Royal Meteorological Society*, *129*(587), 19–38. https://doi.org/10.1256/qj.01.203

Korolev, A. V., Strapp, J. W., Isacc, G. A., & Nevzorov, A. N. (1998). The Nevzorov Airborne Hot-Wire LWC-TWC Probe: Principle of Operation and Performance Characteristics. *Journal of Atmospheric and Oceaninc Technology*, *15*(6), 1495–1510. https://doi-org.ezproxy.library.und.edu/10.1175/1520-0426(1998)015<1495:TNAHWL>2.0.CO;2

Lance, S., Brock, C. A., Rogers, D., & Gordon, J. A. (2010). Water droplet calibration of the Cloud Droplet Probe (CDP) and in-flight performance in liquid, ice and mixed-phase clouds during ARCPAC. *Atmospheric*

*Measurement Techniques*, *3*(6), 1683–1706. https://doi.org/10.5194/amt-3-1683-2010

Lawson, R. P., O'Connor, D., Zmarzly, P., Weaver, K., Baker, B., Mo, Q., & Jonsson, H. (2006). The 2D-S (Stereo) Probe: Design and Preliminary Tests of a New Airborne, High-Speed, High-Resolution Particle Imaging Probe. *Journal of Atmospheric and Oceanic Technology*, *23*(11), 1462–1477. https://doi.org/10.1175/JTECH1927.1

Lilie, L. E., Bouley, D. B., Sivo, C. P., Ratvasky, T. P., & Van Zante, J. F. (2021). *Test Results for the SEA Ice Crystal Detector (ICD) under SLD Conditions at the NASA IRT*. p.2654.

Lilie, L. E., Emery, E., Strapp, J. W., & Emery, J. (2005, January). *A Multiwire Hot-Wire Device for Measurement of Icing Severity, Total Water Content, Liquid Water Content, and Droplet Diameter*. 43rd AIAA Aerospace Sciences Meeting and Exhibit, Reno, Nevada, American Institute of Aeronautics and Astronautics. https://arc.aiaa.org/doi/pdf/10.2514/6.2005-859

Lilie, L. E., Sivo, C. P., & Bouley, D. B. (2016). *Description and Results for a Simple Ice Crystal Detection System for Airborne Applications*. 4058.

McMurdie, L. (2020). *IMPACTS Field Campaign Data Collection* [dataset]. NASA Global Hydrometeorology Resource Center Distributed Active Archive Center. https://doi.org/10.5067/IMPACTS/DATA101

McMurdie, L. A., Heymsfield, G. M., Yorks, J. E., Braun, S. A., Skofronick-Jackson, G., Rauber, R. M., Yuter, S., Colle, B., McFarquhar, G. M., Poellot, M., Novak, D. R., Lang, T. J., Kroodsma, R., McLinden, M., Oue, M., Kollias, P., Kumjian, M. R., Greybush, S. J., Heymsfield, A. J., … Nicholls, S. (2022). Chasing Snowstorms: The Investigation of Microphysics and Precipitation for Atlantic-Coast Threatening Snowstorms (IMPACTS) Campaign. *Bulletin of the American Meteorological Society*, *103*(5), 1243–1269. https://doi-org.ezproxy.library.und.edu/10.1175/BAMS-D-20-0246.1

Merceret, F. J., & Schricker, T. L. (1975). A New Hot-Wire Liquid Cloud Water Meter. *Journal of Applied Meteorology*, *14*(3), 319–326. https://doi.org/10.1175/1520-0450(1975)014<0319:ANHWLC>2.0.CO;2

Personne, P., Brenguier, J. L., Pinty, J. P., & Pointin, Y. (1982). Comparative Study and Calibration of Sensors for the Measurement of the Liquid Water Content of Clouds with Small Droplets. *Journal of Applied Meteorology and Climatology*, *21*(2), 189–196. https://doi.org/10.1175/1520-0450(1982)021<0189:CSACOS>2.0.CO;2

Sandvik, A., Biryulina, M., Kvamstø, N. G., Stamnes, J. J., & Stamnes, K. (2007). Observed and simulated microphysical composition of arctic clouds: Data properties and model validation. *Journal of Geophysical Research: Atmospheres*, *112*(D5). https://doi.org/10.1029/2006JD007351

Science Engineering Associates. (n.d.). *Total Water Content SEA Model WCM-3000 Operating Manual* [Manual]. https://www.scieng.com/pdf/WCM3000OperatingManual.pdf

Strapp, J. W., Oldenburg, J., Ide, R., Lilie, L., Bacic, S., Vukovic, Z., Oleskiw, M., Miller, D., Emery, E., & Leone, G. (2003). Wind Tunnel Measurements of the Response of Hot-Wire Liquid Water Content Instruments to Large Droplets. *Journal of Atmospheric and Oceanic Technology*, *20*(6), 791–806. https://doi.org/10.1175/1520-0426(2003)020<0791:WTMOTR>2.0.CO;2

# APPENDIX A:

# AIRCRAFT QUALITY ASSURANCE PROCEDURES

Quality assurance is done after field project post processing is complete. Quality assurance is done to remove incorrect data points. For instruments such as the hot-wire probes, there is often a spike at the beginning/end of the flight due to the instrument being turned on/off. This is a known issue in the data, so it is removed. Depending on flight procedures during field projects, some flights may begin data collection on the ground before take-off. These issues can be seen in the data at the beginning and end of flight where the true air speed (TAS) gets below 50 knots (25 $ms^{-1}$). These issues are addressed in quality assurance by replacing the incorrect measurement with missing value codes. Use files with TAS (.impacts) to determine take-off and landing times if applicable.

| Instrument | File | Measurements |
|---|---|---|
| King | .analog.raw | LWC |
| WCM-3000 | .seriald1.wcm3000.raw | LWC |
| CDP | .conc.cdp.raw | LWC |
| RICE | .serial.icingMS.raw | IceMSOFreq |

*Making Edits*

$ addedit start=’time in sfm’ end=’time in sfm’ id=’your name’ why=’reason for edit’ filedate.filename.edits filedate.filename.raw

$ apply_edits (file).seriald1.wcm3000.raw (file).edits (file).clean